NASA Contractor Report

RELIABILITY-BASED FAILURE ANALYSIS OF BRITTLE MATERIALS

Lynn M. Powers and Louis J. Ghosn
Cleveland State University
Cleveland, Ohio

February 1989

Prepared for
Lewis Research Center
Under Grant NCC-3-46

RELIABILITY-BASED FAILURE ANALYSIS OF BRITTLE MATERIALS

ABSTRACT

by

Lynn M. Powers and Louis J. Ghosn

The reliability of brittle materials under a generalized state of stress is analyzed using the Batdorf model. The model is modified to include the reduction in shear due to the effect of the compressive stress on the microscopic crack faces. The combined effect of both surface and volume flaws is included. Due to the nature of fracture of brittle materials under compressive loading, the component is modeled as a series system in order to establish bounds on the probability of failure.

A computer program was written to determine the probability of failure employing data from a finite element analysis. The analysis showed that for tensile loading a single crack will be the cause of total failure but under compressive loading a series of microscopic cracks must join together to form a dominant crack.

TABLE OF CONTENTS

LIST OF TABLES

LIST OF FIGURES

FIGURE PAGE

FIGURE PAGE

FIGURE PAGE

CHAPTER I

INTRODUCTION

The demand for high-temperature structural materials has increased due to the growth in the aerospace, defense and energy related industries. Because of the attractive physical and mechanical properties of modern ceramics: high-temperature strength, lightweight, excellent erosion, corrosion and wear resistance, and low thermal conductivity, ceramic components are being considered for structural applications. Examples of these high-temperature applications include: turbine engine components, rocket nozzles and nose tips, nuclear fuel pellets and bearings.

As is the case for other brittle materials, ceramics exhibit a large variation in fracture stress which must be taken into account in design. This variation in strength results from the presence of microscopic random imperfections or flaws. Ceramic components contain two types of flaws: volume flaws and surface flaws. Volume flaws arise from material processing while surface flaws arise from grinding and other surface finishing operations.

Most of the probabilistic approaches to brittle fracture are formulated for tensile failure.[1] However, brittle materials react distinctly under different loading conditions.[2] These materials tend to be weak in tension, but strong in compression. This behavior would suggest that two different failure mechanisms govern the fracture of brittle materials when in tension or in compression. The purpose of this research was to develop a probabilistic model to determine the reliability of brittle materials accounting for the two mechanisms of fracture and which may be applied to any given loading condition, in particular contact stress conditions where the stresses are predominately compressive.

A. Reliability Theory

Reliability is given as the probability of an object performing its required function for a specific period of time under stated conditions. When considering the failure of materials, reliability is measured as the ability of a component to sustain load. The statistical nature of fracture may be presented in two different theories: the weakest link and bundle models.[3] These two concepts are illustrated in Fig. 1.

The weakest link theory makes the analogy between the links of a chain and the volume elements of a bulk specimen. The strength of the chain is that of its weakest link, the strength of the bulk specimen is that of its weakest volume

SERIES SYSTEM – WEAKEST LINK MODEL

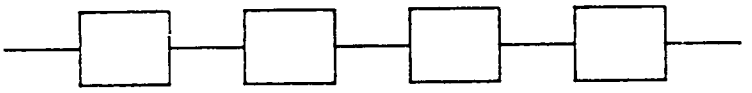

PARALLEL SYSTEM – BUNDLE MODEL

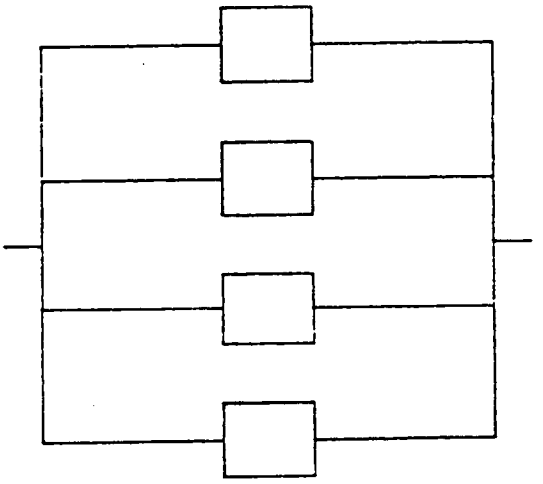

Fig. 1.1 System configuration.

element.[4,5] The strength of its weakest volume element is characterized by its most severe crack. The weakest link theory implies that when one crack fractures the entire specimen fails, representative of a series system.

The alternate concept is that of a bundle model or a parallel system.[6] The volume elements within the material are composed of links arranged in parallel. When one of the links fails, the load is redistributed and the structure may survive. Failure is defined when all of the links have failed.

B. Probabilistic Models For Brittle Fracture

The probabilistic models to be considered are those concerned with the instantaneous fracture as a result of unstable crack propagation when an initial load is applied. Fast fracture of structural components is generally assumed to depend on some property of the material from which the part was made. It is assumed that brittle materials contain microcracks which are uniformly distributed and randomly oriented.

The probabilistic models for brittle fracture are based on the weakest link concept, because one crack almost always produces total failure in tension. The first of these was introduced by Weibull.[4,5] Weibull assumed that the component of stress normal to the plane of the crack was the only one to contribute to its fracture. As a result the shape of the crack is irrelevant and crack-crack interaction

is not taken into account. The statistical distribution function was given as

$$\sigma > \sigma_u \qquad P_f = 1 - \exp\left[- \int_v \left[\frac{\sigma - \sigma_u}{\sigma_o}\right]^m dv \right] \qquad 1.1$$

$$\sigma \leq \sigma_u \qquad = 0$$

where the probability of failure, P_f, is a function of the maximum principal tensile stress and three material constants: m, σ_o and σ_u, the Weibull modulus, scaling factor and the threshold stress, respectively. A similar distribution for surface flaws may be written by integrating over the area instead of the volume. An example of this probability distribution is shown in Fig. 2. This theory was initially used for materials under uniform tension and was extended[7] for non-uniform uniaxial stress states.

The flaw density distribution characterized by the material constants in the Weibull analysis may be difficult to determine.[8] A unique combination of values for the three parameters does not exist within the range used for experimental data, $0.05 < P_f < 0.95$. For a single data set the difference between various fits will be small in this range but large in the extrapolated region at the lower tail of the distribution where the probability of failure necessary for design is located. For simple stress states the distribution of flaws may be obtained without assuming any functional form.[9] Matthews' theory was extended for

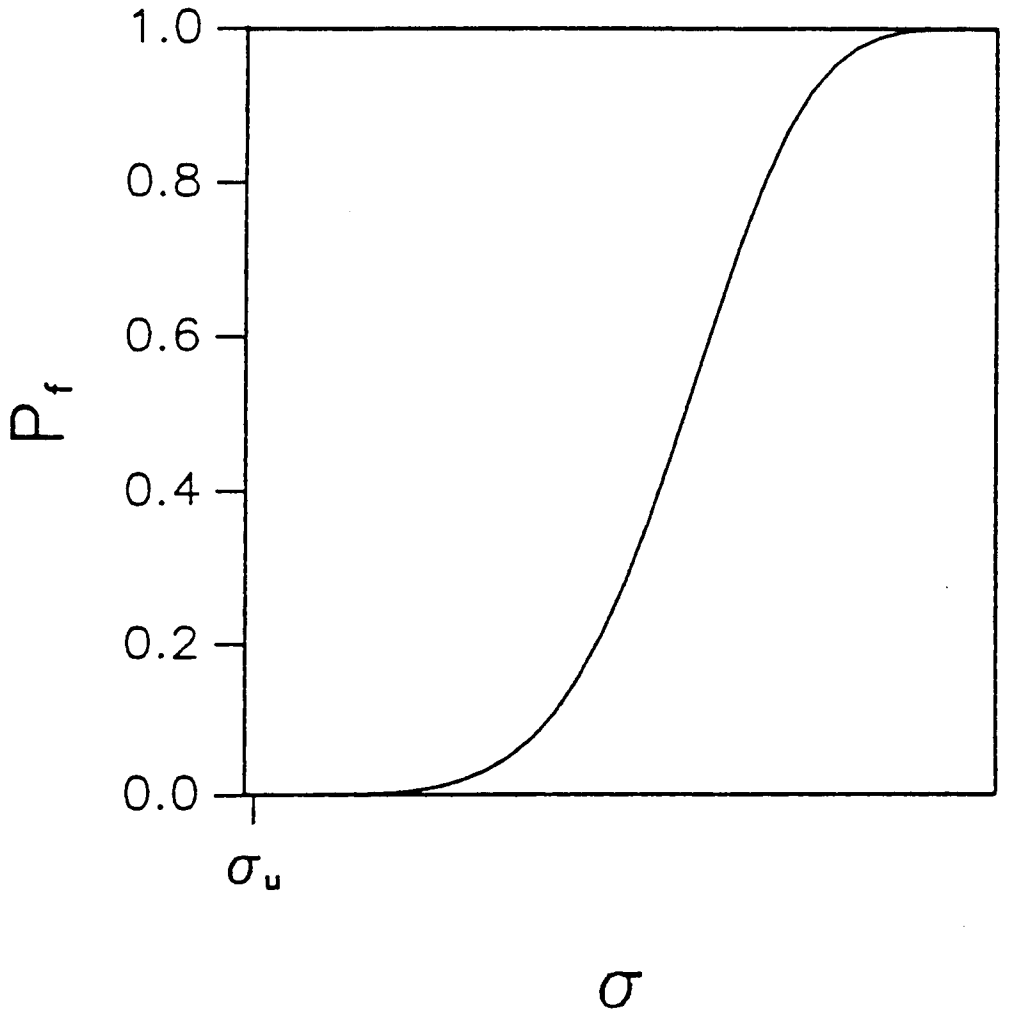

Fig. 1.2 Weibull's distribution function.

biaxial configurations by Evans.[10] However for multiaxial states of stress, a flaw density distribution must be extrapolated for untested regions.[11]

To further apply Weibull theory to polyaxial states of stress, the Principal of Independent Action (PIA) was developed.[12] The PIA hypothesis states that the probability of survival is equal to the product of the survival probabilities for each of the three principal stresses individually. The probability of failure is given as:

$$P_f = 1 - \exp\left[- \int_V \left[\frac{\sigma_1}{\sigma_o}\right]^m + \left[\frac{\sigma_2}{\sigma_o}\right]^m + \left[\frac{\sigma_3}{\sigma_o}\right]^m dv \right] \qquad 1.2$$

where σ_1, σ_2 and σ_3 are the principal stresses. This method will yield unconservative estimates of stress because all nonzero principal stresses contribute to the stress normal to the plane of the flaw.[13]

The Batdorf model,[14] accounts for this by including a stress space integral inside of Weibull's volume/surface integral. Batdorf's assumption that these flaws are cracks will combine Weibull's statistical model with fracture mechanics theory. Material failure is now associated with crack growth. Since both normal and shear stresses contribute to crack growth, an appropriate fracture criterion is needed to account for combined loading.[15] The presence of shear reduces the normal stress needed to produce fracture.

This occurs when the stress on the crack reaches a critical value which is a function of the fracture criterion and the crack configuration. Two of the mixed-mode fracture criteria which have been used in combination with the Batdorf model are the maximum tensile strength and the strain-energy release rate, for volume cracks[16] and for surface cracks.[17]

Arbitrarily stressed components may be analyzed by dividing them into small volumes of material whose stress state is assumed constant. Stress analysis using the finite element method is compatible with this model to determine the failure probability.[18]

C. Brittle Fracture In Compression

In general, the models mentioned thus far do not include the effect of compressive normal stresses on the crack. However, Griffith introduced the idea that brittle materials fracture in compression. In a material containing pre-existing cracks, the unequal principal compressive forces generate shear stresses which act against frictional forces producing tensile stresses near the crack tip.[19] The crack branches nearly parallel to the direction of maximum compression. This secondary crack will grow until the tension at the crack tip has dropped to the applied compression.[20] This effect is illustrated in Fig. 3.

Since the existing cracks are microscopic, a single crack does not produce total failure as it almost always

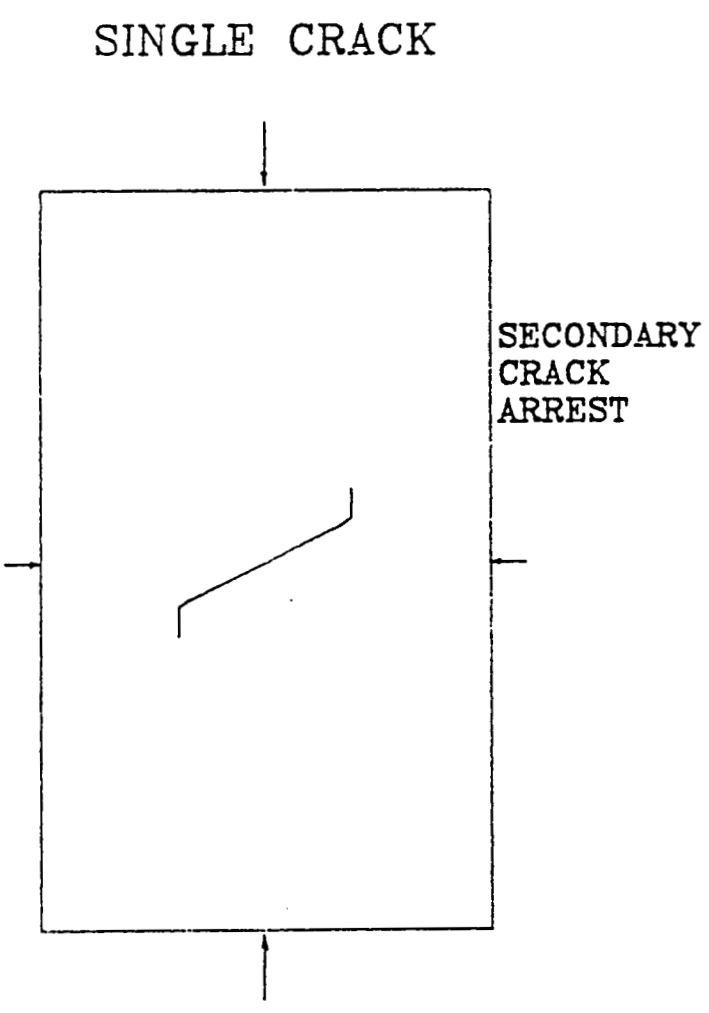

Fig. 1.3 Crack growth under compressive loading.

does in tension. Total fracture occurs when several of these cracks extend and join together creating a shear fault.[21] Compressive failure is dependent on the total flaw distribution not on the weakest flaw alone.[22] Using the weakest link concept, initiation of fracture of a single crack has been predicted,[23] for specific stress states however, crack interaction was not considered.

D. Thesis Outline

The purpose of this study is to model the behavior of brittle materials under arbitrary loading conditions. This program uses data from a finite element analysis to determine the probability of failure originating from volume and/or surface flaws. Due to the nature of the fracture of brittle materials under compression, the component is modeled as a series system in order to establish bounds on the probability of failure. When the material is represented in this manner crack-crack interaction is taken into account.

In Chapter II, the Batdorf model for failure prediction in tension is presented. The material is assumed to contain a distribution of uniformly distributed and randomly oriented cracks. The failure strength of a material with pre-existing cracks is determined from experimental data using the 4-point bend test.

In Chapter III, the modified Batdorf model for compressive loading is developed. The reduction in shear

due to the effect of the compressive stress on the crack face is included in the analysis for volume and surface flaws.

The calculation of the bounds on the probability of failure is described in Chapter IV. An element is equivalent to a component in the system. Determination of the probability of failure for an element is shown based on the stress output from the finite element analysis.

In Chapter V, the model is applied to determine the probability of failure for contact stress problems. The thesis concludes with Chapter VI, where the results and conclusions of the study are presented. The needs for future research are given.

CHAPTER II

FRACTURE PREDICTION

The failure of brittle materials has been attributed to the presence of flaws. The material fails when the strength of the weakest flaw is exceeded. These flaws were assumed to be cracks whose strength was dependent on their size and orientation.[14] Batdorf assumed that these cracks were uniformly distributed and randomly oriented as shown in Fig. 2.1. The material will fail when the effective stress on a crack reaches a critical value σ_{cr} characteristic of that particular crack. To determine the effective stress σ_e, the shape and the fracture criterion must be assumed.

Two of the mixed-mode fracture criteria which have been used with the Batdorf model are the maximum tensile strength and the strain-energy release rate. The strain-energy release rate was selected for this analysis because of its greater degree of shear-sensitivity. The effective stress applied on a crack is given as:[16]

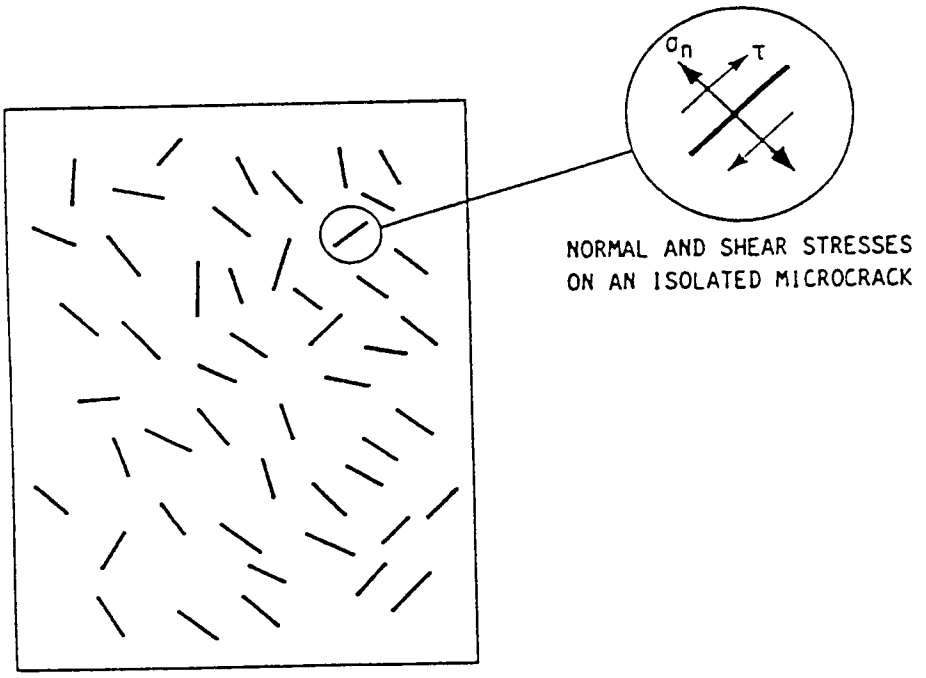

Fig. 2.1 Random crack distribution in brittle materials.

$$\sigma_e = \sqrt{\sigma_n^2 + \tau^2} \qquad 2.1$$

for a Griffith crack, where σ_n is the macroscopic tensile stress normal to the plane of the crack and τ is the shear parallel to it. A crack will fracture when the effective stress is greater than the critical stress. In the σ_n-τ plane eq. 2.1 is a boundary outside of which a crack will initiate fracture. This boundary is referred to as the fracture envelope.

A. Surface Flaw Analysis

When a crack is lying on the surface of a material, it is assumed that stresses present only at the surface contribute to its growth. As a result the crack is subjected to plane stress conditions. The two principal stresses on the surface are σ_{1a} and σ_{3a}, because they will represent the maximum and minimum principal stresses on the plane. The stress perpendicular to the surface will not effect the growth of surface cracks, however it is included in the volume flaw analysis. The subscript a implies a surface quantity.

To determine the probability of failure, the surface is divided into elements. Within each element the stress state is assumed constant. The probability of failure for surface cracks may be expressed[24] as:

$$P_{fa} = P_{1a}P_{2a} \tag{2.2}$$

where P_{1a} is the probability of existence in the element of surface area of a crack having a critical stress in the range σ_{cr} to $\sigma_{cr} + d\sigma_{cr}$ and P_{2a} is the probability that a crack will be oriented so that the effective stress is greater than or equal to the critical stress. P_{1a} has the form

$$P_{1a} = \Delta A \frac{dN_a(\sigma_{cr})}{d\sigma_{cr}} d\sigma_{cr} \tag{2.3}$$

where ΔA is the area of the element and $N_a(\sigma_{cr})$ is the surface crack density function which is defined as the number of cracks per unit area having a critical stress greater than or equal to σ_{cr}. The crack density function is material dependent and is assumed to be

$$N_a = k_{Ba}\sigma_{cr}^{m_a} \tag{2.4}$$

where k_{Ba} and m_a are determined experimentally.

P_{2a} is given as:

$$P_{2a} = \bar{\omega} = \frac{\omega}{\pi/2} \tag{2.5}$$

where ω is the radian measure of the angular range in the quadrant of stress space within which the effective stress

is greater than or equal to σ_{cr}. The total angular range in this region is $\frac{\pi}{2}$. When $\sigma_{ea} \geq \sigma_{cr}$ over the entire range, then $\omega = \frac{\pi}{2}$. If $\sigma_{ea} < \sigma_{cr}$ everywhere, then $\omega = 0$. The probability that a crack will be oriented so that $\sigma_{ea} \geq \sigma_{cr}$, is $0 \leq P_{2a} \leq 1$.

The overall probability of failure is:

$$P_{fa} = 1 - \exp\left[-\int_A dA \int_0^{\sigma_{1a}} \frac{dN_a(\sigma_{cr})}{d\sigma_{cr}} \bar{\omega}\, d\sigma_{cr} \right] \qquad 2.6$$

for the entire area A. The limits on the integration of σ_{cr} are a consequence of the assumed crack density function and the stress state. When $\sigma_{cr} \leq 0$ the quantity P_{1a} as given in eq. 2.3 is equal to zero. P_{2a} is zero if $\sigma_{cr} \geq \sigma_{1a}$ because the effective stress is never greater than σ_{1a} when all of the principal stresses are tensile.

When the crack density function is known, the only quantity needed to calculate the probability in eq. 2.6 is $\bar{\omega}$, a function of the stress state and the fracture criterion. For a crack on the surface of the material, the fracture criterion given in eq. 2.1 is stated as;

$$\sigma_{ea} = \sqrt{\sigma_{na}^2 + \tau_a^2} \qquad 2.7$$

where σ_{ea} is the effective stress acting on a surface crack and σ_{na} and τ_a are the normal and shear stresses on a crack.

The magnitude of the traction vector $|\sigma_a|$, is:

$$|\sigma_a|^2 = \sigma_{1a}^2\cos^2\beta + \sigma_{3a}^2\sin^2\beta \qquad 2.8$$

where β is the angle between the σ_{1a}-axis and the crack normal.

The normal and shear stresses are respectively given as:

$$\sigma_{na} = \sigma_{1a}\cos^2\beta + \sigma_{3a}\sin^2\beta \qquad 2.9$$

$$\tau_a = \sqrt{|\sigma_a^2| - \sigma_{na}^2} \qquad 2.10$$

Substituting eqs. 2.9 and 2.10 into eq. 2.7 gives an expression for the effective stress,

$$\sigma_{ea}^2 = \sigma_{3a}^2 + (\sigma_{1a}^2-\sigma_{3a}^2)\cos^2\beta \qquad 2.11$$

$\sigma_{cr} \geq \sigma_{ea}$ over the range $0 \leq \beta \leq \beta_{cr}$, then

$$\beta_{cr} = \cos^{-1}\left[\frac{\sigma_{cr}^2 - \sigma_{3a}^2}{\sigma_{1a}^2 - \sigma_{3a}^2}\right]^{1/2} \qquad 2.12$$

Since $\omega = \beta_{cr}$

$$\bar{\omega} = 1 \qquad \sigma_{cr} \leq \sigma_{3a}$$

$$\bar{\omega} = \frac{2}{\pi} \cos^{-1} \left[\frac{\sigma_{cr}^2 - \sigma_{3a}^2}{\sigma_{1a}^2 - \sigma_{3a}^2} \right]^{1/2} \qquad \sigma_{3a} < \sigma_{cr} \leq \sigma_{1a} \qquad 2.13$$

Fig. 2.2 shows the angle ω as a representation of the arc of Mohr's circle outside the fracture envelope as given in eq. 2.7.

B. Volume Flaw Analysis

Within an element of volume whose stress state is assumed constant, the probability of failure may be written:[24]

$$P_{fv} = P_{1v} P_{2v} \qquad 2.14$$

where P_{1v} is the probability of existence in the element of volume of a crack having a critical stress in the range σ_{cr} to $\sigma_{cr} + d\sigma_{cr}$ and P_{2v} is the probability that a crack will be oriented so that the effective stress is greater than or equal to the critical stress. The subscript v will be used to define volume quantities. P_{1v} has the form

$$P_{1v} = \Delta V \frac{dN_v(\sigma_{cr})}{d\sigma_{cr}} d\sigma_{cr} \qquad 2.15$$

where ΔV is the volume of the element and $N_v(\sigma_{cr})$ is the crack density function which is defined as the number of

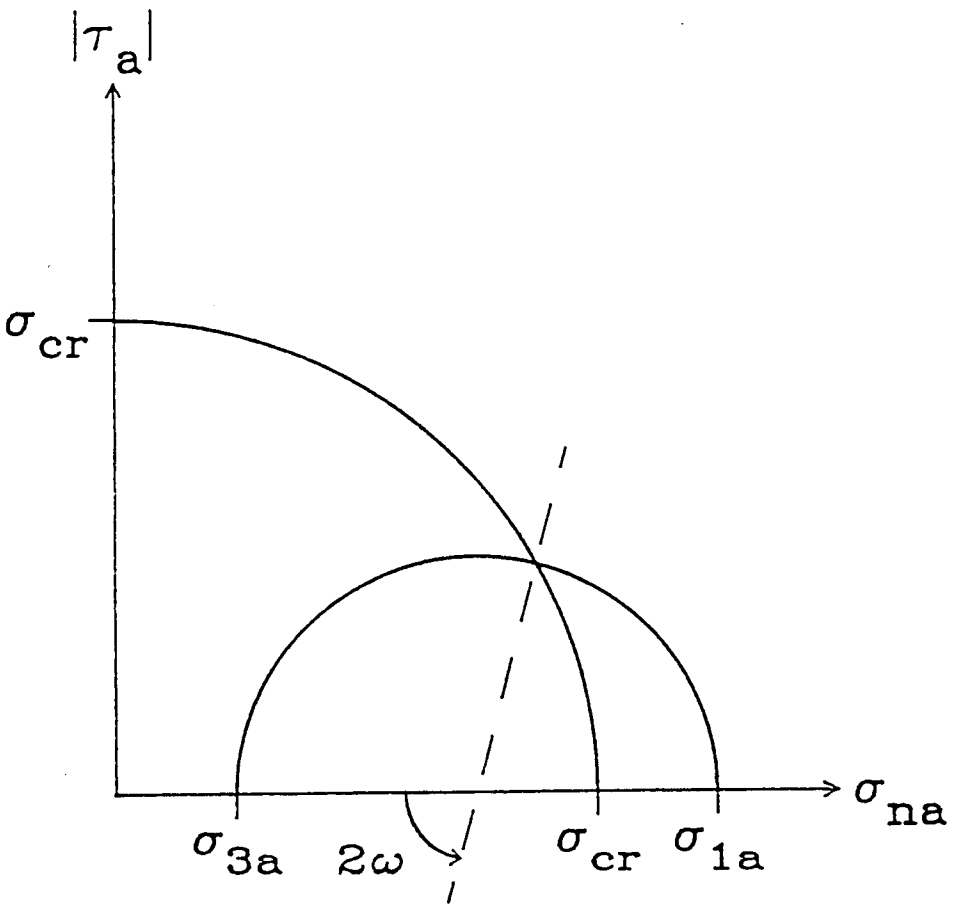

Fig. 2.2 The angle ω represented by the arc of Mohr's circle outside the fracture envelope.

cracks per unit volume having a critical stress greater than or equal to σ_{cr}. The crack density function is material dependent and is assumed to be

$$N_v = k_{Bv}\sigma_{cr}^{m_v} \qquad 2.16$$

where k_{Bv} and m_v are determined experimentally.

P_{2v} is given as:

$$P_{2v} = \bar{\Omega} = \frac{\Omega}{4\pi} \qquad 2.17$$

where Ω is the solid angle on a unit sphere containing all of the orientations for which $\sigma_{ev} \geq \sigma_{cr}$. The overall probability of failure is:

$$P_{fv} = 1 - \exp\left[-\int_V dV \int_0^{\sigma_{1v}} \frac{dN_v(\sigma_{cr})}{d\sigma_{cr}} \bar{\Omega}\, d\sigma_{cr} \right] \qquad 2.18$$

for the volume V. The limits on the integration of σ_{cr} are similar to those used in eq. 2.6. The only quantity needed to calculate the probability of failure is $\bar{\Omega}$, a function of the stress state and the fracture criterion. For a crack inside the volume of material, the fracture criterion given in eq. 2.1 is stated as:

$$\sigma_{ev} = \sqrt{\sigma_{nv}^2 + \tau_v^2} \qquad 2.19$$

where σ_{ev} is the effective stress acting on a volume crack and σ_{nv} and τ_v are the normal and shear stresses on the crack.

A normal to the plane of the crack is defined as shown in Fig. 2.3, in principal stress space where $\sigma_{1v} \leq \sigma_{2v} \leq \sigma_{3v}$. α is the angle between the normal and the σ_{2v}-axis and β is the angle between the normal and the σ_{1v}-axis in a plane perpendicular to the intermediate principal stress. The direction cosines are

$$\begin{aligned} l &= \sin \alpha \cos \beta \\ m &= \cos \alpha \\ n &= \sin \alpha \sin \beta \end{aligned} \qquad 2.20$$

The magnitude of the traction on the plane is:

$$|\sigma_v|^2 = \sigma_{1v}^2 l^2 + \sigma_{2v}^2 m^2 + \sigma_{3v}^2 n^2 \qquad 2.21$$

the normal and shear are

$$\sigma_{nv} = \sigma_{1v} l^2 + \sigma_{2v} m^2 + \sigma_{3v} n^2 \qquad 2.22$$

$$\tau_v = \sqrt{|\sigma_v^2| - \sigma_{nv}^2} \qquad 2.23$$

Substituting eq. 2.20 into eq. 2.21

$$|\sigma_v|^2 = \sigma_{3v}^2 + (\sigma_{1v}^2 - \sigma_{3v}^2)\sin^2\alpha \cos^2\beta + (\sigma_{2v}^2 - \sigma_{3v}^2)\cos^2\alpha \qquad 2.24$$

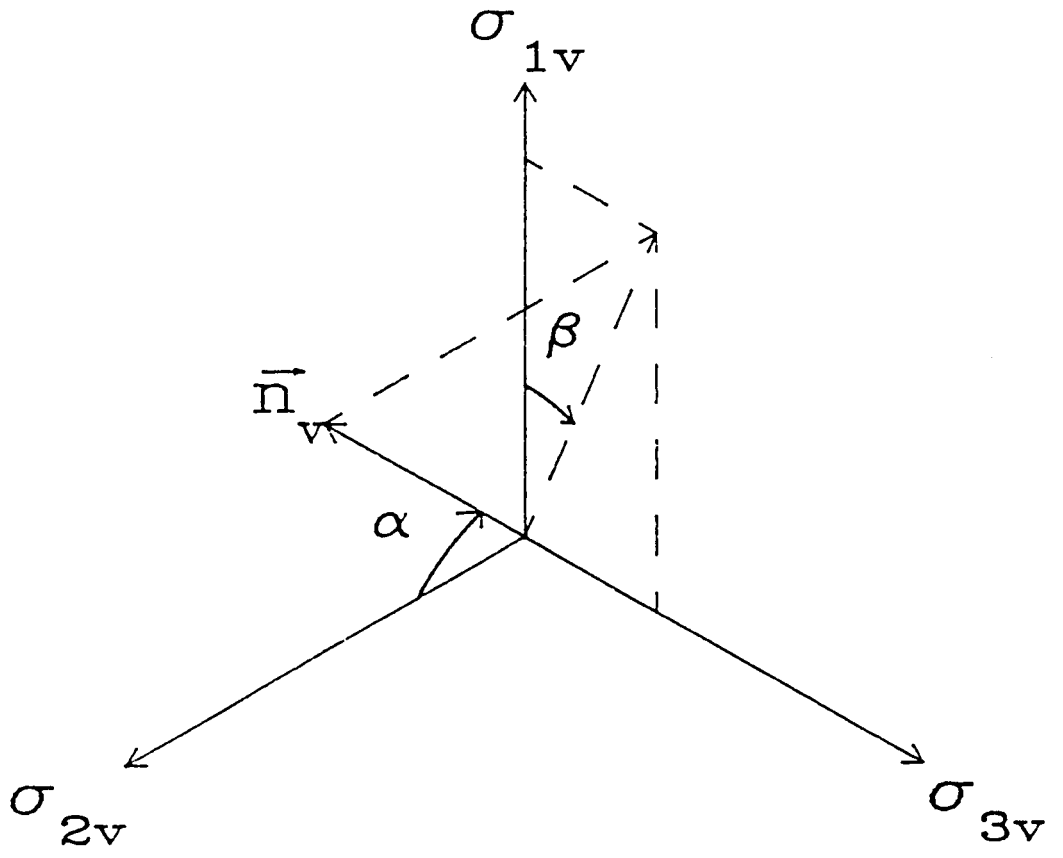

Fig. 2.3 The orientation of the normal to a crack plane in principal stress space.

and similarly for the normal stress in eq. 2.22

$$\sigma_{nv} = \sigma_{3v} + (\sigma_{1v}-\sigma_{3v})\sin^2\alpha\,\cos^2\beta + (\sigma_{2v}-\sigma_{3v})\cos^2\alpha \qquad 2.25$$

Originally,[14] P_{2v} was determined in the following manner. The fracture criterion in eq. 2.19 may be stated using the traction vector

$$\sigma_{ev} = |\sigma_v| \qquad 2.26$$

then eq. 2.24 is of the form

$$a\delta^2 + b\delta + c = 0$$

where $\delta = \cos^2\beta$, then

$$a = 0$$

$$b = (\sigma_{1v}^2-\sigma_{3v}^2)\,\sin^2\alpha$$

$$c = (\sigma_{2v}^2-\sigma_{3v}^2)\,\cos^2\alpha + \sigma_{3v}^2 - \sigma_{cr}^2$$

Using the quadratic formula, δ is determined. Let $\overline{\beta} = \cos^{-1}\sqrt{\delta}$ then

$$\overline{\Omega} = \frac{1}{\pi}\int_0^{\pi} \overline{\beta}\,\sin\alpha\,d\alpha \qquad 2.27$$

If $\delta \leq 0$, $\bar{\beta} = \frac{\pi}{2}$ which indicates that the effective stress is greater than or equal to σ_{cr} everywhere for the angle α. Also if $\delta > 1$, $\bar{\beta} = 0$ or $\sigma_{ev} < \sigma_{cr}$ everywhere for the angle α.

The calculation of P_{2v} in eq. 2.27 is simplified if two planes tangent to the unit sphere at A and B are defined as shown in Fig. 2.4. Their normals are

$$\begin{aligned} \vec{n}_A &= \sin\alpha\, \mathbf{i} + \cos\alpha\, \mathbf{j} \qquad \beta = 0 \\ \vec{n}_B &= \cos\alpha\, \mathbf{j} + \sin\alpha\, \mathbf{k} \qquad \beta = \pi/2 \end{aligned} \tag{2.28}$$

where i, j and k are the unit vectors in the σ_{1v}, σ_{2v} and σ_{3v} directions, respectively. The traction on A and B

$$\begin{aligned} |\sigma_A|^2 &= \sigma_{1v}^2 - (\sigma_{1v}^2 - \sigma_{2v}^2)\cos^2\alpha \\ |\sigma_B|^2 &= \sigma_{3v}^2 + (\sigma_{2v}^2 - \sigma_{3v}^2)\cos^2\alpha \end{aligned} \tag{2.29}$$

then the traction as given in eq. 2.24 is written:

$$|\sigma_v|^2 = |\sigma_B|^2 + (|\sigma_A|^2 - |\sigma_B|^2)\cos^2\beta \tag{2.30}$$

The normal stresses on A and B are

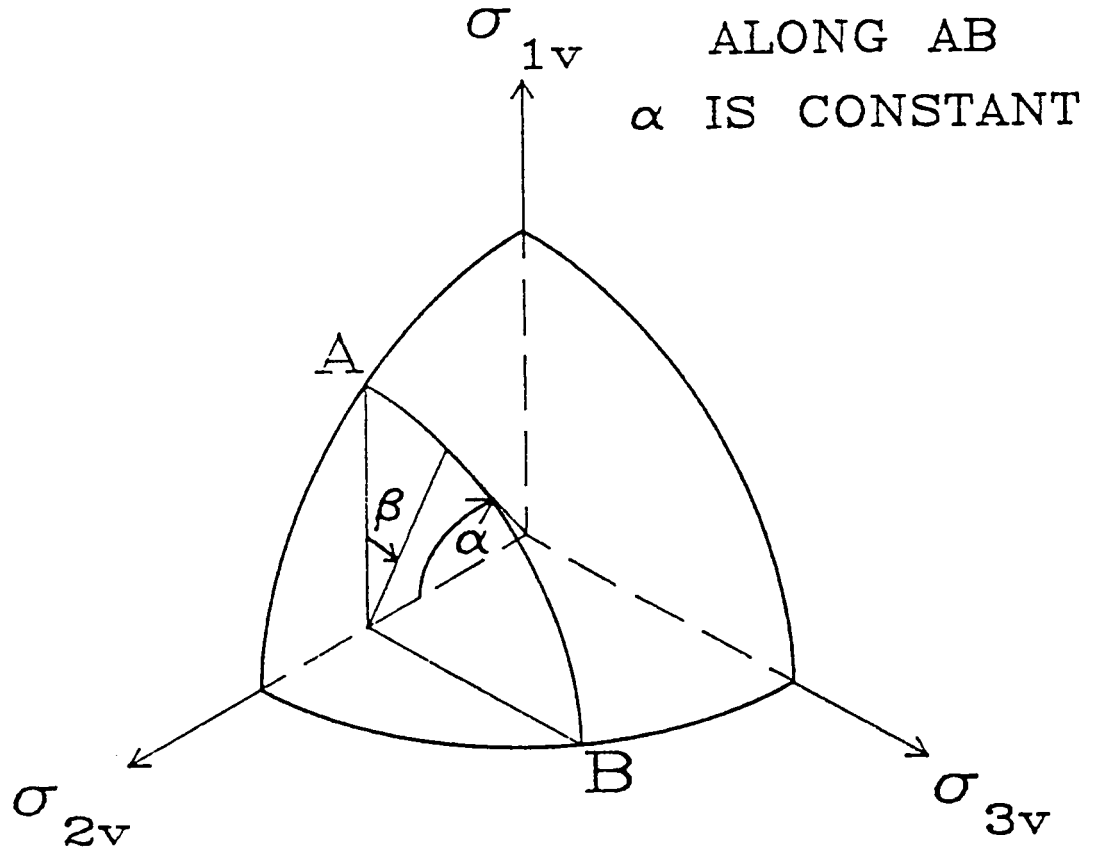

Fig. 2.4 The location of points A and B on a unit sphere in principal stress space.

$$\sigma_{nA} = \sigma_{1v} - (\sigma_{1v}-\sigma_{2v})\cos^2\alpha$$

$$\sigma_{nB} = \sigma_{3v} + (\sigma_{2v}-\sigma_{3v})\cos^2\alpha \qquad 2.31$$

and the normal stress on any plane is:

$$\sigma_{nv} = \sigma_{nB} + (\sigma_{nA}-\sigma_{nB})\cos^2\beta \qquad 2.32$$

P_{2v} may be determined by substituting eq. 2.30 into eq. 2.26

$$\sigma_{cr}^2 = |\sigma_B|^2 + (|\sigma_A|^2 - |\sigma_B|^2)\cos^2\beta_{cr} \qquad 2.33$$

then

$$\beta_{cr} = \cos^{-1}\left[\frac{\sigma_{cr}^2 - |\sigma_B|^2}{|\sigma_A|^2 - |\sigma_B|^2}\right]^{1/2} \qquad 2.34$$

where β_{cr} is a function of σ_{cr}, $|\sigma_A|$, $|\sigma_B|$ and implicitly α. Eq. 2.34 is similar to eq. 2.12 for surface cracks. As was the case for surface cracks, $\sigma_{ev} \geq \sigma_{cr}$ over $o \leq \beta \leq \beta_{cr}$, or $\omega = \beta_{cr}$. Eq. 2.27 may be written:

$$\bar{\Omega} = \int_0^{\pi/2} \bar{\omega} \sin\alpha \, d\alpha \qquad 2.35$$

where

$$\bar{\omega} = 0 \qquad |\sigma_A| \leq \sigma_{cr}$$

$$\bar{\omega} = \frac{2}{\pi} \cos^{-1} \left[\frac{\sigma_{cr}^2 - |\sigma_B|^2}{|\sigma_A|^2 - |\sigma_B|^2} \right]^{1/2} \qquad |\sigma_B| < \sigma_{cr} < |\sigma_A| \qquad 2.36$$

$$\bar{\omega} = 1 \qquad \sigma_{cr} \leq |\sigma_B|$$

where $|\sigma_A|$ and $|\sigma_B|$ are given by eq. 2.29 as a function of α. The region inside Mohr's circle of stress which lies outside the fracture envelope represents orientations within which a crack must lie to initiate fracture as shown in Fig 2.5. An example of the solid angle Ω on a unit sphere is shown in Fig. 2.6.

C. Determination Of Material Parameters

The crack density functions, N_a and N_v, contain two constants which must be determined experimentally. A plot of the probability of failure versus the fracture stress is made from the data and is fitted to:

$$P_f = 1 - \exp \left[-k\sigma_f^m \right] \qquad 2.37$$

where σ_f is the fracture stress, k and m are determined using the least squares method.

Given a fracture theory, an expression for the probability of failure can be found which is a function of the specimen geometry and loading conditions. This expression is used in combination with eq. 2.37 to evaluate

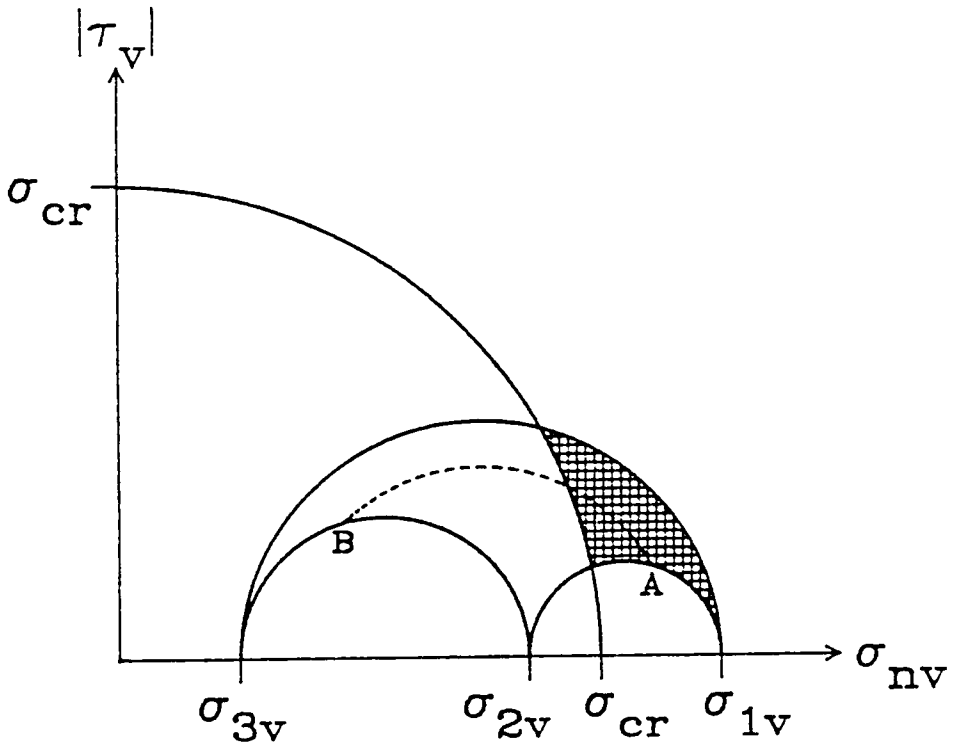

Fig. 2.5 Orientation of cracks which will initiate fracture on Mohr's circle of stress.

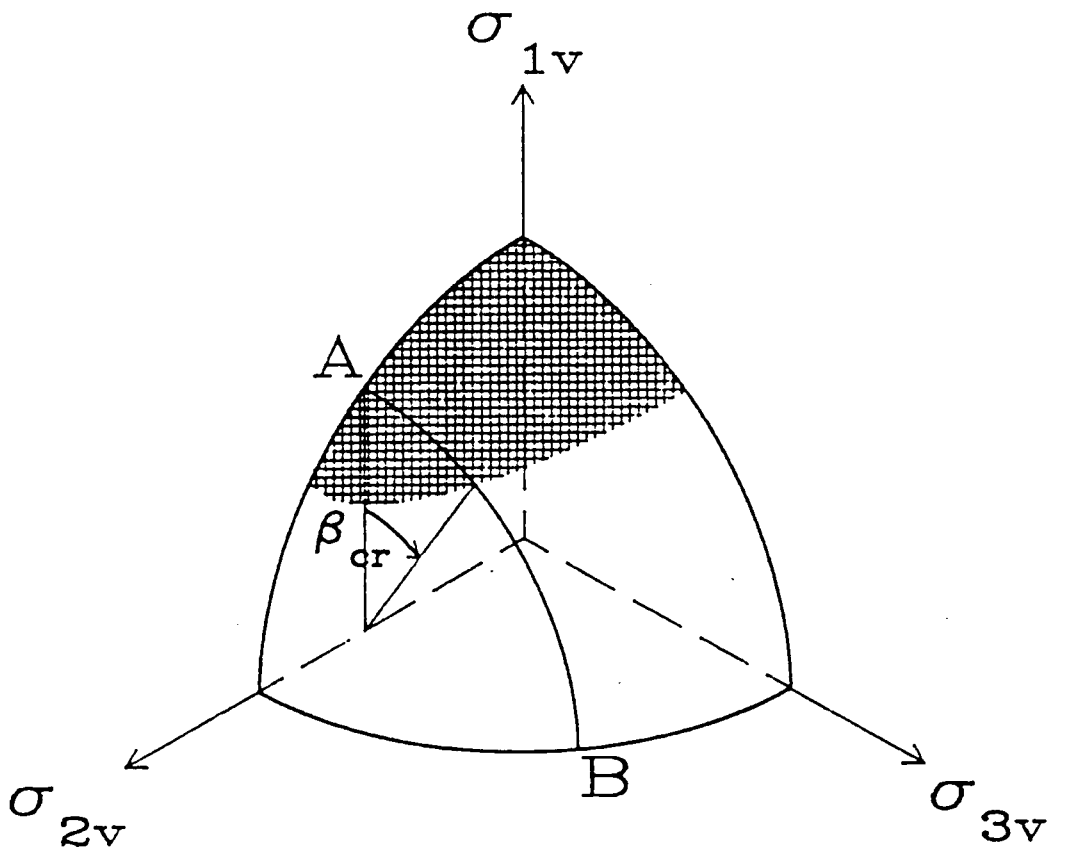

Fig. 2.6 Solid angle within which cracks must be oriented to initiate fracture on a unit sphere.

the material parameters. Ideally, a uniform tension test would be the easiest to formulate. However, this test is not popular because the ceramic tensile specimens are costly and their load train is not easily aligned. The four-point bend test has become the preferred test because it can be controlled and the stress field is uniaxial but not uniform. The test configuration is shown in Fig. 2.7 for a beam with a circular cross-section.

The stress distribution in the beam as a function of the maximum tensile stress is given by

$$\sigma = \frac{2\sigma_{max}}{(L_o - L_i)\ R} \times r \sin\theta \qquad 0 \le x \le (L_o - L_i)/2$$

$$\sigma = \frac{\sigma_{max}}{R} r \sin\theta \qquad (L_o - L_i)/2 \le x \le (L_o + L_i)/2 \qquad 2.38$$

$$\sigma = \frac{2\sigma_{max}}{(L_o - L_i)\ R} (L_o - x)\ r \sin\theta \qquad (L_o + L_i)/2 \le x \le L_o$$

where R is the radius of the beam, L_o is the distance between the outer loads, L_i is the distance between the inner loads and σ_{max} is the magnitude of the maximum tensile stress in the beam. $\sigma = \sigma_{max}$ between the inner loads and at $\theta = \frac{\pi}{2}$. Since the magnitude of the tensile stresses and the compressive stresses are equal, the beam will most likely fail in tension.

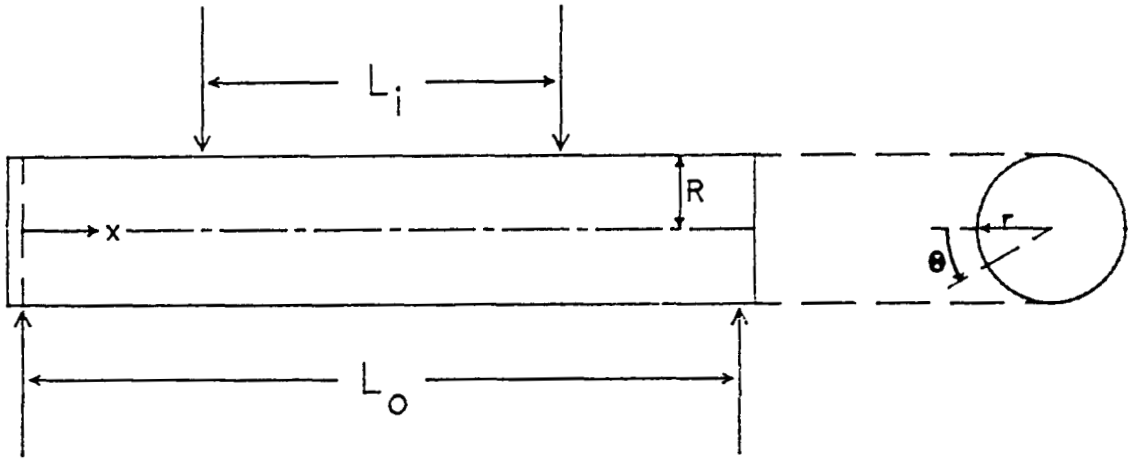

Fig. 2.7 A beam of circular cross-section with four point loads.

1. Surface Flaws

For a uniaxial state of stress with $\sigma_{1a} = \sigma$, and $\sigma_{3a} = 0$ the probability that a crack will be oriented so the effective stress is greater than or equal to the critical stress is:

$$\bar{\omega} = \frac{2}{\pi} \cos^{-1} \left[\frac{\sigma_{cr}}{\sigma} \right] \qquad 2.39$$

substituting eq. 2.39 into eq. 2.6

$$P_{fa} = 1 - \exp \left[-\int_A \int_0^{\sigma} \frac{2}{\pi} \cos^{-1} \left[\frac{\sigma_{cr}}{\sigma} \right] \frac{dN_a(\sigma_{cr})}{d\sigma_{cr}} \, d\sigma_{cr} \, dA \right] \qquad 2.40$$

If it assumed that when $\sigma_{cr} = 0$, then $N_a = 0$, eq. 2.40 is integrated by parts and substituting eq. 2.4 into eq. 2.40

$$P_{fa} = 1 - \exp \left[-\int_A \int_0^{\sigma} \frac{2k_{Ba}\sigma_{cr}^{m_a}}{\pi\{\sigma^2 - \sigma_{cr}^2\}^{1/2}} \, d\sigma_{cr} \, dA \right] \qquad 2.41$$

Let

$$\eta = \left[\frac{\sigma_{cr}}{\sigma} \right]^2$$

then

$$P_{fa} = 1 - \exp\left[-\int_A \frac{k_{Ba}\sigma^{m_a}}{\pi} Z \, dA \right] \qquad 2.42$$

where

$$Z = \int_0^1 \eta^{\left[\frac{m_a-1}{2}\right]} \{1-\eta\}^{-1/2} \, d\eta \qquad 2.43$$

Integrating eq. 2.42 over the tensile portion of the beam

$$P_{fa} = 1 - \exp\left[-\int_0^{\pi} \int_0^{L_o} \frac{Zk_{Ba}\sigma^{m_a}}{\pi} R \, dx \, d\theta \right] \qquad 2.44$$

and substituting eq. 2.38 into eq. 2.44 gives an expression for the probability of failure in terms of the specimen geometry and the loading conditions

$$P_{fa} = 1 - \exp\left[- \frac{ZRk_{Ba}(L_o+m_aL_i)\ \sigma_{max}^{m_a}}{\pi(m_a+1)} \int_0^{\pi} \sin^{m_a}\theta \, d\theta \right] \qquad 2.45$$

The constants k_{Ba} and m_a are determined by equating the exponents in eq. 2.45 and eq. 2.37

$$m_a = m \qquad 2.46$$

$$k_{Ba} = \frac{\pi(m_a+1)k}{ZR(L_o+m_aL_i)\int_0^{\pi} \sin^{m_a}\theta \, d\theta} \qquad 2.47$$

where σ_{max} is the fracture stress, σ_f.

2. Volume Flaws

For a uniaxial state of stress with $\sigma_{1v} = \sigma$, and $\sigma_{2v} = \sigma_{3v} = 0$ the probability that a crack will be oriented so the effective stress is greater than or equal to the critical stress can be computed directly[18]

$$\bar{\Omega} = 1 - \frac{\sigma_{cr}}{\sigma} \qquad 2.48$$

substituting eq. 2.48 into eq. 2.10

$$P_{fv} = 1 - \exp\left[-\int_V \int_0^{\sigma} \left[1 - \frac{\sigma_{cr}}{\sigma}\right] \frac{dN_v(\sigma_{cr})}{d\sigma_{cr}} \, d\sigma_{cr} \, dV \right] \qquad 2.49$$

substituting eq. 2.16 into eq. 2.49 and integrating over σ_{cr}

$$P_{fv} = 1 - \exp\left[-\int_V \frac{k_{Bv}}{(m_v+1)} \sigma^{m_v} \, dV \right] \qquad 2.50$$

Integrating eq. 2.50 over the tensile portion of the beam

$$P_{fv} = 1 - \exp\left[-\int_0^{\pi} \int_0^{R} \int_0^{L_o} \frac{k_{Bv}}{(m_v+1)} \sigma^{m_v} \, r \, dx \, dr \, d\theta \right] \qquad 2.51$$

and substituting eq. 2.38 into eq. 2.51 gives an expression for the probability of failure in terms of the specimen geometry and the loading conditions

$$P_{fv} = 1 - \exp\left[- \frac{k_{Bv} \, (L_o+m_v L_i) \, R^2 \, \sigma_{max}^{m_v}}{(m_v+1)^2(m_v+2)} \int_0^{\pi} \sin^{m_v} \theta \, d\theta \right] \qquad 2.52$$

The constants k_{Bv} and m_v are determined by equating the exponents in eq. 2.52 and eq. 2.37

$$m_v = m \qquad 2.53$$

$$k_{Bv} = \frac{(m_v+1)^2(m_v+2) \, k}{(L_o+m_v L_i) \, R^2 \int_0^{\pi} \sin^{m_v} \theta \, d\theta} \qquad 2.54$$

where σ_{max} is the fracture stress, σ_f.

D. Numerical Integration

When the stress state and the crack density function are known, the probability of failure may be calculated. However, numerical integration is necessary to compute the failure probabilities as given in eqs. 2.6 and 2.18. To evaluate these integrals the Gaussian quadrature method is

used. The integration of an arbitrary function over a finite interval may be approximated by

$$\int_a^b f(x)\,dx \approx \frac{b-a}{2} \sum_{i=1}^{N} f\left[x_i\left[\frac{b-a}{2}\right] + \frac{a+b}{2}\right] w_i \qquad 2.55$$

where N is the number of sampling points, x_i and w_i are the location and weight of the ith sampling point, respectively. These values x_i and w_i are tabulated for different numbers of sampling points.[25]

The probability of failure for surface cracks is more efficiently computed[24] if

$$S_a = \frac{\sigma_{cr}}{\sigma_{1a}} \qquad 2.56$$

then substituting eq. 2.4 into 2.6 gives:

$$P_{fa} = 1 - \exp\left[-A m_a k_{Ba} \sigma_{1a}^{m_a} \int_0^1 \bar{\omega}\, S_a^{m_a-1}\, dS_a \right] \qquad 2.57$$

where $\bar{\omega}$ is given by eq. 2.13 or as given by eq. 2.36 where $|\sigma_A| = \sigma_{1a}$ and $|\sigma_B| = \sigma_{3a}$. Applying eq 2.55 to the integral in eq. 2.57 gives:

$$P_{fa} = 1 - \exp\left[\frac{-A m_a k_{Ba} \sigma_{1a}^{m_a}}{2} \sum_{i=1}^{N} \bar{\omega}_i\, \xi_{a_i}^{m_a-1}\, w_i \right] \qquad 2.58$$

where

$$\xi_{a_i} = \frac{x_{a_i}+1}{2}$$

$\bar{\omega}_i$ is evaluated at ξ_{a_i} and x_{a_i} and w_i are tabulated according to the number of sampling points used.

A similar process is utilized to evaluate the probability of failure for volume cracks as given in eq. 2.18. If

$$S_v = \frac{\sigma_{cr}}{\sigma_{1v}} \qquad 2.59$$

then substituting eqs. 2.59 and 2.16 into eq. 2.18 gives:

$$P_{fv} = 1 - \exp\left[-V m_v k_{Bv} \sigma_{1v}^{m_v} \int_0^{\pi/2} \int_0^1 \bar{\omega} \sin \alpha \, S_v^{m_v-1} dS_v \, d\alpha \right] \qquad 2.60$$

where $\bar{\omega}$ is given by eq. 2.36. Applying eq 2.55 to the integral in eq. 2.60 gives:

$$P_{fv} = 1 - \exp\left[\frac{-\pi V m_v k_{Bv} \sigma_{1v}^{m_v}}{8} \sum_{i=1}^{M} \sum_{j=1}^{N} \bar{\omega}_{ij} \sin \zeta_j \, \xi_{v_i}^{m_v-1} \, w_i w_j \right] \qquad 2.61$$

where

$$\xi_{v_i} = \frac{x_{v_i}+1}{2} \qquad \zeta_j = \frac{\pi(x_j+1)}{4}$$

$\bar{\omega}_{ij}$ is evaluated at ξ_{v_i} and ζ_j. x_{v_i}, w_i, x_j and w_j are tabulated as a function of M or N.

It is of interest to note that for both volume and surface analysis the probability of failure is dependent on a common function, $\bar{\omega}$. Therefore in the subsequent analysis of compressive stress states, it is not necessary to consider both volume and surface probabilities but to formulate $\bar{\omega}$ so that it may be used in both eq. 2.58 for surface probability and in eq. 2.61 for the probability of failure for an element of volume.

CHAPTER III

FRACTURE INITIATION UNDER COMPRESSIVE LOADING

Brittle materials with pre-existing cracks may fracture when loaded in compression.[21] The unequal principal compressive stresses generate shear stresses which act against frictional forces, initiating local crack growth. Since the existing cracks are microscopic, a single crack does not produce total failure as it almost always does in tension. Total failure occurs when several of these cracks extend and join together. Before the failure of an entire component can be analyzed, the fracture of a single crack must be considered.

When the stress normal to the crack plane is compressive, the shear and the friction due to the normal stress will act against one another[23]

$$\tau_e = |\tau| + \mu\sigma_n \qquad 3.1$$

where τ_e is the effective shear stress on the crack and μ is the internal friction coefficient of the material. τ_e is defined as the shear stress necessary to initiate fracture

when the normal stress is less than zero.[26]

The criterion given in eq. 3.1 is combined with the strain-energy release rate criterion in eq. 2.1. τ_e must be equal to the value of the effective stress as given in eq. 2.1 when $\sigma_n = 0$, in order to preserve continuity in shear. Then the fracture criterion for $\sigma_n < 0$ is stated:

$$\sigma_e = \tau_e = |\tau| + \mu\sigma_n \qquad 3.2$$

The fracture envelope in shown in Fig. 3.1. Failure probabilities are based on the combination of the two criteria as were given in eqs. 2.1 and 3.2.

To accomodate the new fracture criterion, two modifications are made to the Batdorf model as presented in Chapter II. First, the maximum effective stress σ_{emax}, is not always equal to the maximum principal stress as it did when all of the principal stresses were tensile, resulting in a change in the limits on the integration of σ_{cr} in eqs. 2.6 and 2.18. Second P_2 the probability that the effective stress is greater than or equal to the critical stress, must be reformulated.

The subscript notation used in this and subsequent chapters will not include a reference to a surface or volume flaw analysis. For example, the quantity N refers to both N_a the surface crack density function and N_v the volume crack density function.

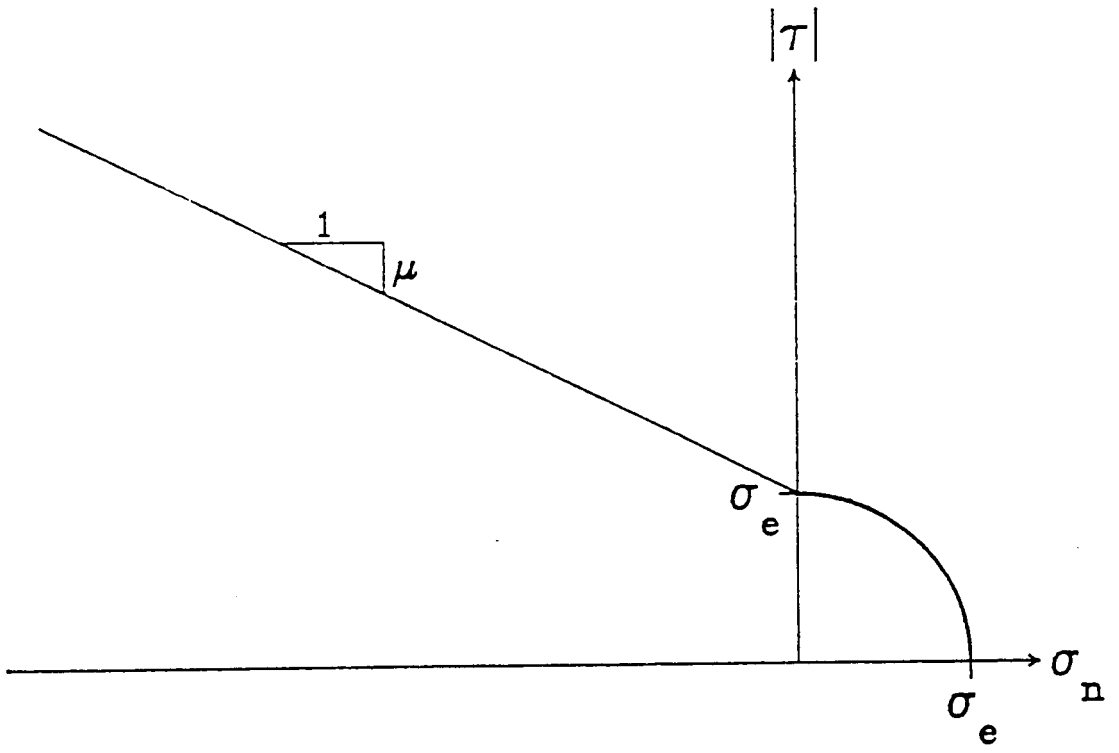

Fig. 3.1 Fracture envelope.

A. Maximum Effective Stress

In order to calculate the effective stress exceeding the critical stress P_2, the effective stress for all crack orientations must be considered. When the critical stress is greater than the maximum effective stress, $P_2 = 0$. In terms of the fracture envelope shown in Fig. 3.1, $\sigma_e = \sigma_{emax}$ when Mohr's circle of stress is tangent to the fracture envelope. The orientation of the normal to the plane on which σ_{emax} acts must lie in the 13-plane.

The maximum effective stress is characterized differently depending upon the nature of the stress on the element.

1. Compression - Mohr's circle is tangent to the linear portion of the fracture envelope
2. Tension - The maximum effective stress is equal to the maximum principal stress.
3. Tension and compression combined - A transition region where σ_{emax} is equal to the shear stress when only shear is present.

The limitations of each of these three methods will be discussed in order to develope a general algorithm for the determination of the maximum effective stress.

1. Compression

Mohr's circle is tangent to the linear portion of the fracture envelope when the effective stress given by eq. 3.3 is a maximum. The normal and shear stresses in the 13-plane are:

$$\sigma_n = \frac{\sigma_1+\sigma_3}{2} + \frac{\sigma_1-\sigma_3}{2} \cos 2\beta$$

$$|\tau| = \frac{\sigma_1-\sigma_3}{2} \sin 2\beta \qquad 3.3$$

where β is the angle between the crack normal and the σ_1-axis. The effective stress in the 13-plane is given by substituting eq. 3.3 into 3.2

$$\sigma_e = \frac{\sigma_1-\sigma_3}{2} \sin 2\beta + \mu\left[\frac{\sigma_1+\sigma_3}{2} + \frac{\sigma_1-\sigma_3}{2} \cos 2\beta\right] \qquad 3.4$$

To determine where σ_{emax} is located, one must find the orientation where the slope

$$\frac{\partial \sigma_e}{\partial \beta} = (\sigma_1-\sigma_3) \cos 2\beta - \mu\,(\sigma_1-\sigma_3) \sin 2\beta$$

is equal to zero. Solving for $\beta = \beta_{max}$, at $\sigma_e = \sigma_{emax}$ one obtains

$$\tan 2\beta_{max} = \frac{1}{\mu} \qquad 3.5$$

which is a function of the internal friction coefficient. Mohr's circle is tangent to the fracture envelope at the point where $\beta = \beta_{max}$ as shown in Fig. 3.2. For the limiting case $\mu = 0$, σ_{emax} occurs at $\beta_{max} = \frac{\pi}{4}$, which is the location of the maximum shear stress.

A general expression for σ_{emax} can be found from eq. 3.5, given by:

$$\sin 2\beta_{max} = \frac{1}{\sqrt{1 + \mu^2}}$$

$$\cos 2\beta_{max} = \frac{\mu}{\sqrt{1 + \mu^2}} \qquad 3.6$$

substituting eq 3.6 into eq. 3.4 gives:

$$\sigma_{emax} = \sqrt{1 + \mu^2}\ \frac{\sigma_1 - \sigma_3}{2} + \mu\ \frac{\sigma_1 + \sigma_3}{2} \qquad 3.7$$

Since $\sigma_1 \geq \sigma_3$, the first term in eq 3.7 is always greater than or equal to zero. However $\sigma_n < 0$ for all β, then $\sigma_1 + \sigma_3 < 0$. If $\sigma_{emax} \leq 0$, the frictional force along the crack is greater than the shear and all cracks under these loading conditions are locked. For example, under hydrostatic pressure $\sigma_3 = \sigma_1 < 0$, no shear is present. This phenomenon also takes place near the orientation of compressive principal stresses.

For any stress state whose maximum effective stress is

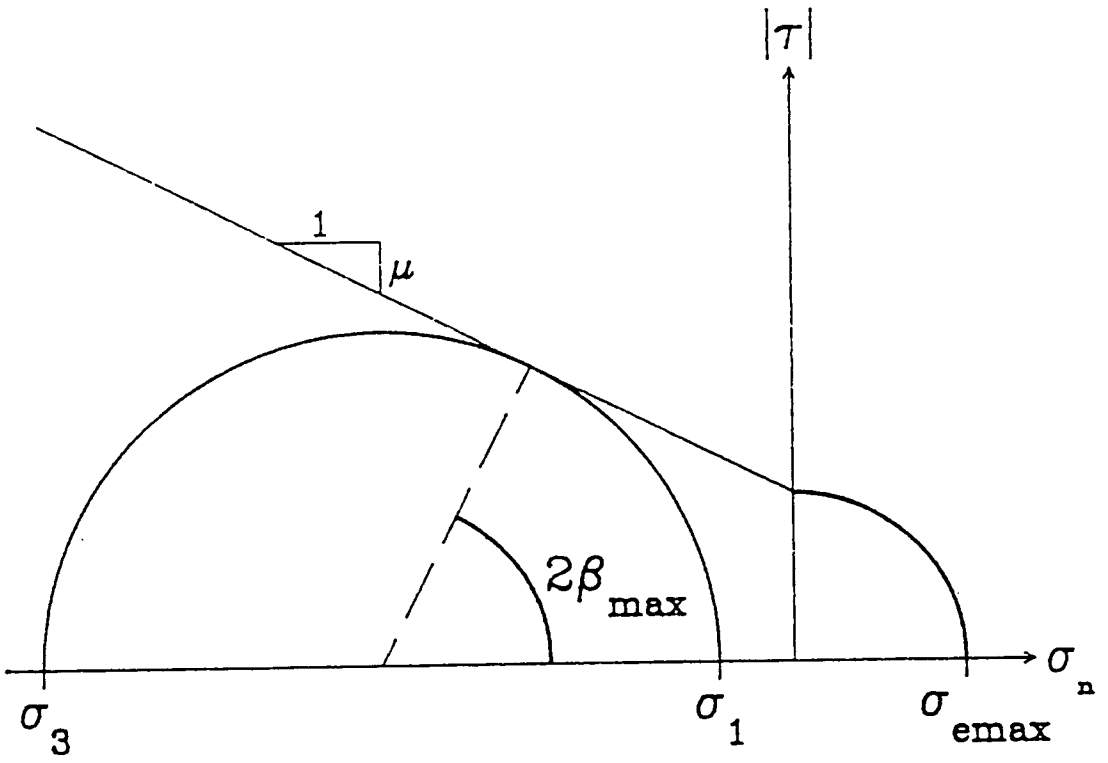

Fig. 3.2 The maximum effective stress as Mohr's circle is tangent to the linear portion of the fracture envelope.

less than or equal to zero, cracks will always lock. The probability of failure for these regions is always equal to zero, therefore they may be eliminated from the overall analysis. This is done by considering the ratio of minimum to maximum principal stress:

$$R = \frac{\sigma_3}{\sigma_1}$$

when $\sigma_3 \leq \sigma_1 < 0$, $R \geq 1$ because the magnitude of σ_3 is greater than or equal to the magnitude of σ_1. When $\sigma_{emax} = 0$, $R = R_0$ then from eq. 3.7

$$R_0 = \frac{(1+\mu^2)^{1/2} + \mu}{(1+\mu^2)^{1/2} - \mu} \qquad 3.8$$

Fig. 3.3 shows the crack locking region in the σ_n-τ plane with Mohr's circle at $R = R_0$.

R_0 as a function of the internal friction coefficient is shown in Fig. 3.4. If $1 \leq R \leq R_0$ the maximum effective stress is less than zero and all cracks will lock. The elements whose principal stress ratio falls in this range are eliminated from the failure analysis.

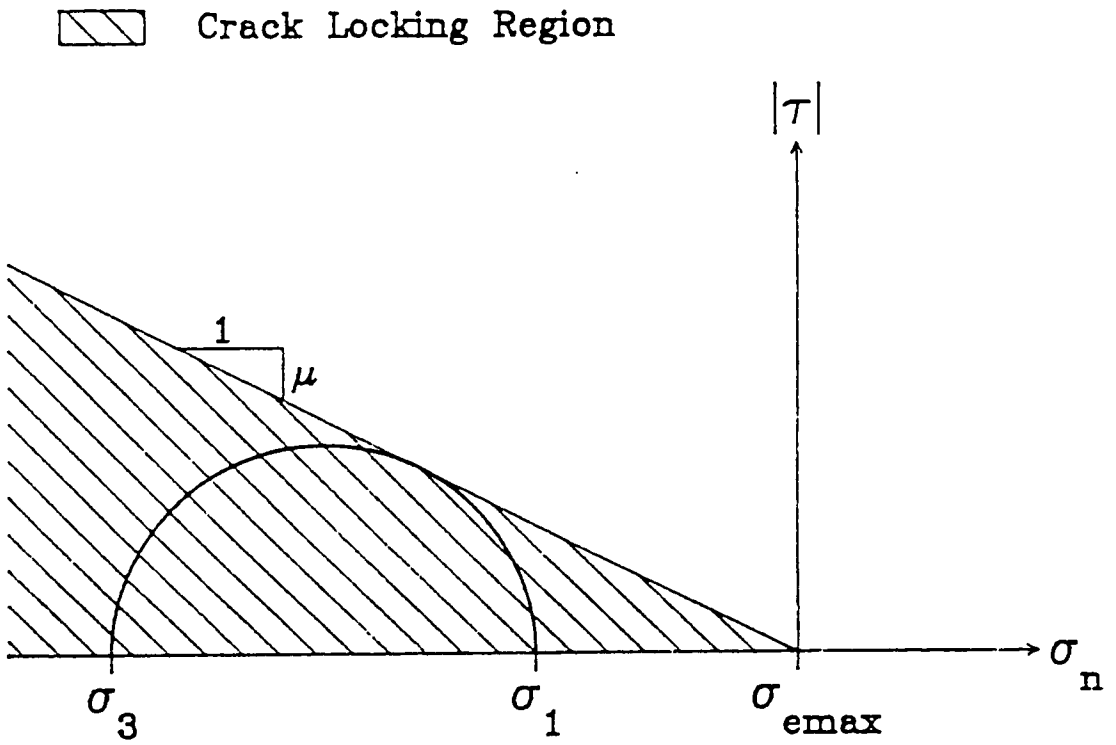

Fig. 3.3 Mohr's circle when the maximum effective stress is equal to zero.

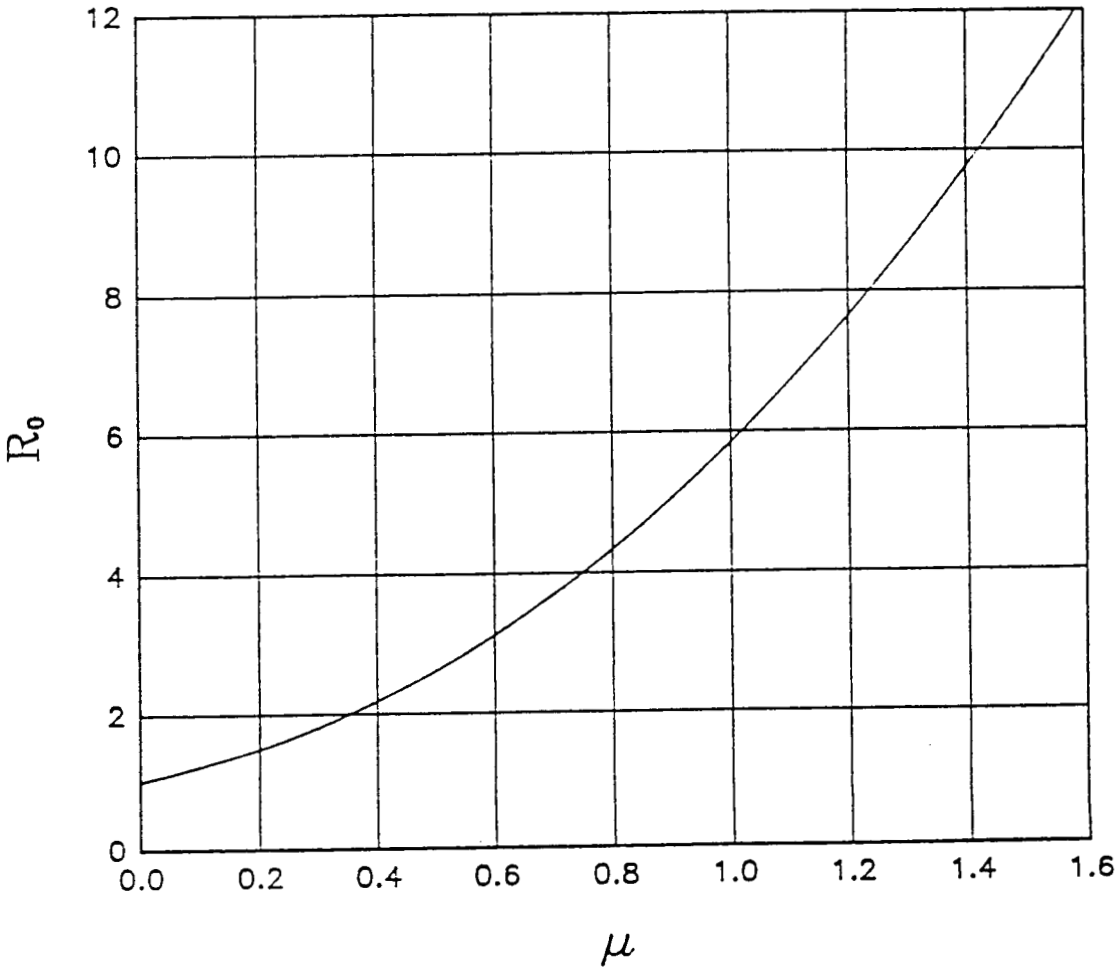

Fig. 3.4 The principal stress ratio as a function of the internal friction coefficient when the maximum effective stress is equal to zero.

2. Tension

When the normal stress is greater than or equal to zero everywhere or $0 \leq \sigma_3 \leq \sigma_1$, σ_{emax} is determined using the strain-energy release rate fracture criteria. As was discussed in Chapter II, the maximum effective stress is equal to the maximum principal stress. Mohr's circle is tangent to the fracture envelope at $\sigma_n = \sigma_1$ as shown in Fig. 3.5.

3. Tension and compression combined

The maximum effective stress has been determined if the normal stress is either tensile or compressive for any crack orientation. When $\sigma_3 < 0 < \sigma_1$, both of the fracture criteria must be considered to find σ_{emax}. The value of σ_{emax} is governed by:

a. Compressive criterion.

b. A transition region between tensile and compressive criteria.

c. Tensile criterion.

depending on the ratio of minimum to maximum principal stress.

a. Compressive criteria.

The maximum effective stress will be located at $\beta = \beta_{max}$ as long as the normal stress at that orientation is compressive. The normal stress at the orientation of maximum effective stress, $\beta = \beta_{max}$ is given by eq. 3.3:

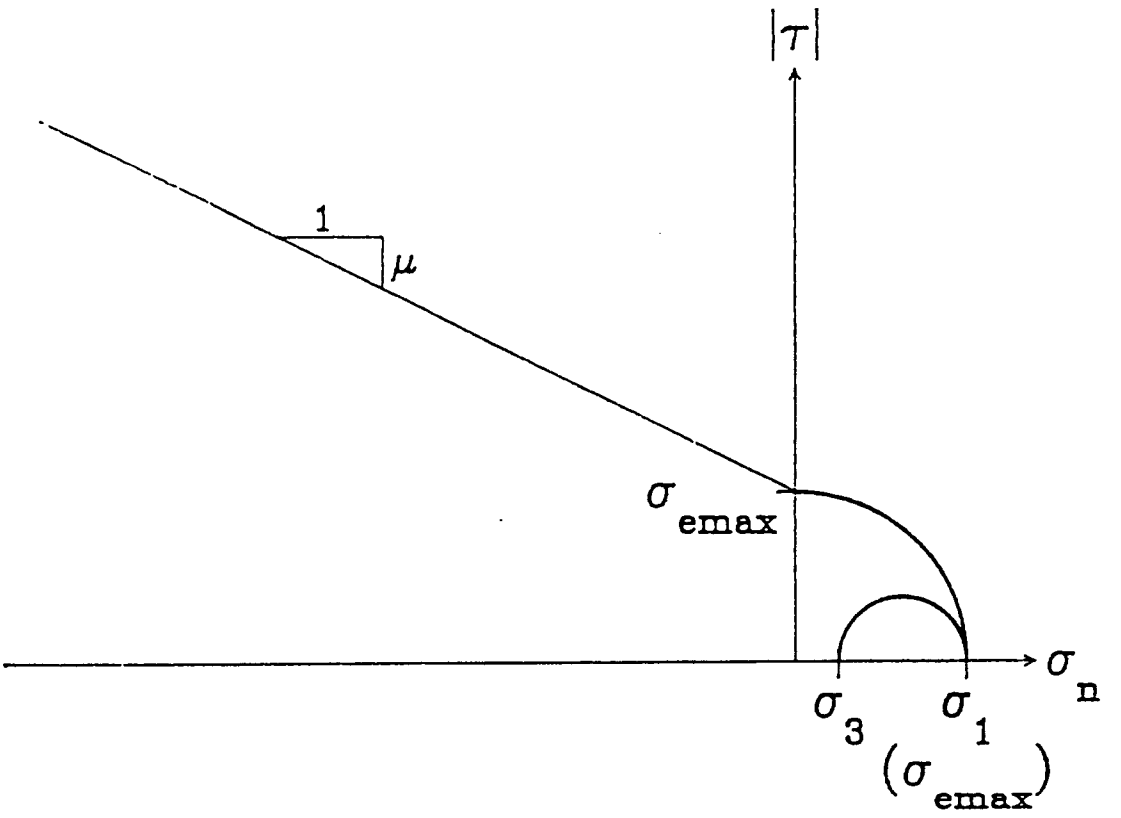

Fig. 3.5 The maximum effective stress is equal to the maximum principal stress.

$$\sigma_n = \frac{\sigma_1+\sigma_3}{2} + \frac{\sigma_1-\sigma_3}{2} \cos 2\beta_{max} \qquad 3.9$$

To determine when the normal stress changes from compressive to tensile, let $\sigma_n = 0$ and substitute eq. 3.6 into 3.9 which gives:

$$\frac{\sigma_3}{\sigma_1} = - \frac{(1+\mu^2)^{1/2} + \mu}{(1+\mu^2)^{1/2} - \mu} = -R_0 \qquad 3.10$$

where R_0 is defined as the principal stress ratio when $\sigma_{emax} = 0$. If $R \leq -R_0$ the maximum effective stress is given by eq. 3.7 because $\sigma_n < 0$ at β_{max}, or Mohr's circle is tangent to the linear portion of the fracture envelope as shown in Fig. 3.6.

b. The transition between tensile and compressive criteria

If the normal stress at $\beta = \beta_{max}$ is tensile the maximum effective stress may occur at the angle which separates the tensile and compressive fields or $\sigma_n = 0$. Let $\beta = \beta_0$ at $\sigma_n = 0$ from eq. 3.6

$$2\beta_0 = \cos^{-1} -\left[\frac{\sigma_1+\sigma_3}{\sigma_1-\sigma_3}\right] \qquad 3.11$$

then the shear is:

$$\sigma_{emax} = \tau_0 = \frac{\sigma_1-\sigma_3}{2} \sin 2\beta_0 \qquad 3.12$$

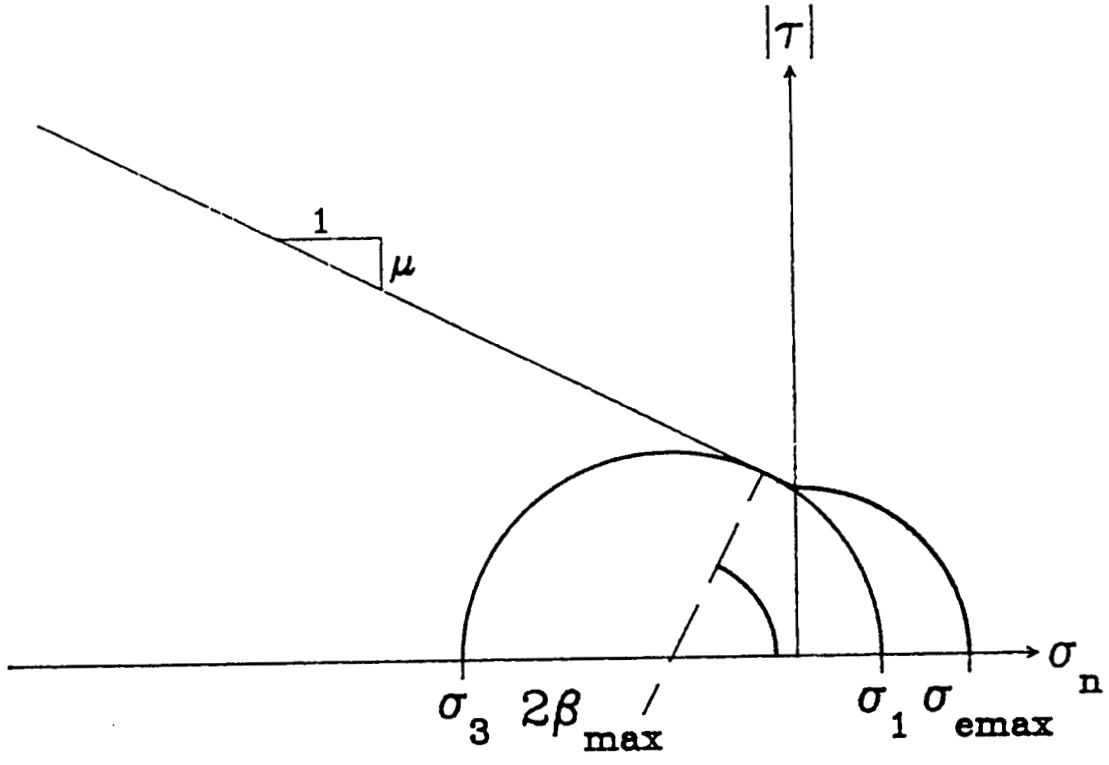

Fig. 3.6 The maximum effective stress as Mohr's circle is tangent to the linear portion of the fracture envelope with a tensile principal stress.

where τ_0 is the magnitude of the shear stress at $\sigma_n = 0$. Fig. 3.7 shows an example of a state of stress where $\sigma_{emax} = \tau_0$. The maximum effective stress will be equal to τ_0 as long as $\tau_0 > \sigma_1$. $\tau_0 = \sigma_1$, if $\sigma_1 = -\sigma_3$, then $\sigma_{emax} = \tau_0$ over the range: $-R_0 \leq R \leq -1$.

c. Tensile criterion.

When the tensile stress dominates, the maximum effective stress is equal to σ_1 as it does when σ_n is always tensile. For $|\sigma_3| \leq \sigma_1$, $\sigma_{emax} = \sigma_1$ as shown in Fig. 3.8. A summary of the maximum effective stress for different stress states is given in Table 3.1.

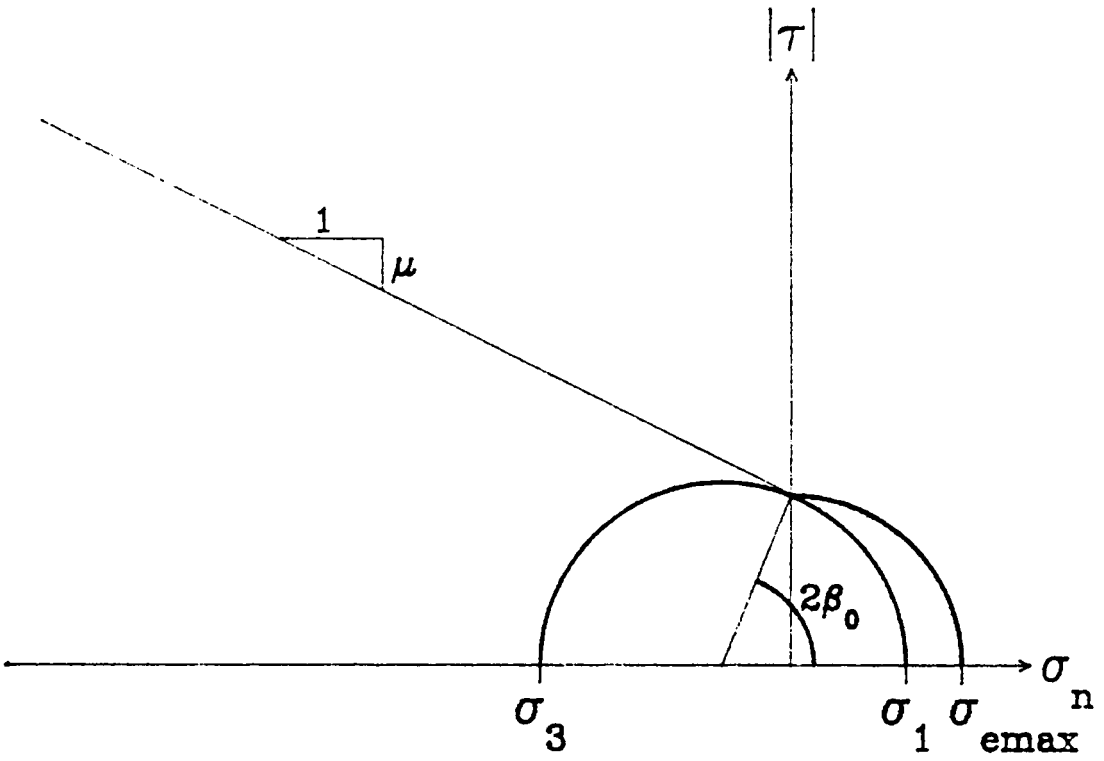

Fig. 3.7 The maximum effective stress as Mohr's circle is tangent to the the fracture envelope at $\sigma_n = 0$.

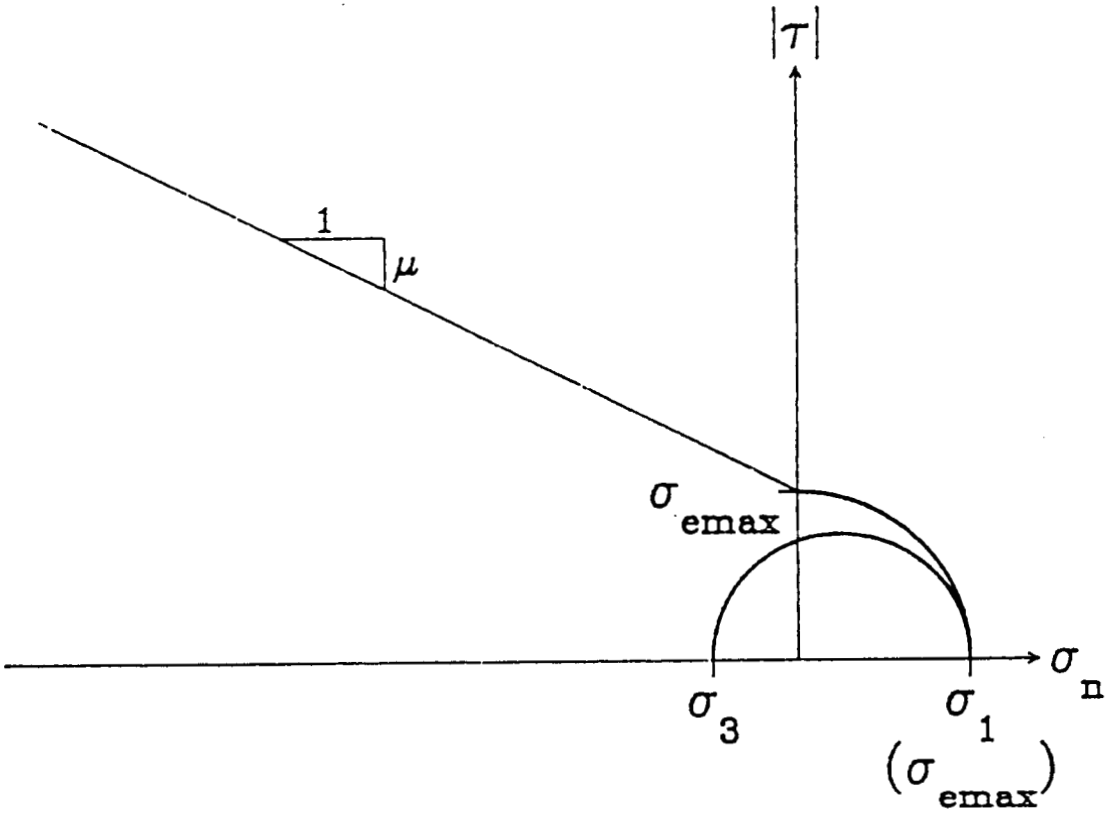

Fig. 3.8 The maximum effective stress equal to the maximum principal stress.

Table 3.1 The maximum effective stress for ratios of principal stress.

Stress State	σ_{emax}	Illustration
1. $0 \leq \sigma_3 \leq \sigma_1$	σ_1	Fig. 3.5
2. $\sigma_3 < 0 < \sigma_1$		
$\lvert\sigma_3\rvert \leq \sigma_1$	σ_1	Fig. 3.8
$-R_0 < \frac{\sigma_3}{\sigma_1} < -1$	τ_0	Fig. 3.7
$\frac{\sigma_3}{\sigma_1} \leq -R_0$	$\sqrt{1+\mu^2}\,\frac{\sigma_1-\sigma_3}{2} + \mu\,\frac{\sigma_1+\sigma_3}{2}$	Fig. 3.6
3. $\sigma_3 \leq \sigma_1 < 0$		
$R_0 < \frac{\sigma_3}{\sigma_1}$	$\sqrt{1+\mu^2}\,\frac{\sigma_1-\sigma_3}{2} + \mu\,\frac{\sigma_1+\sigma_3}{2}$	Fig. 3.2
$\frac{\sigma_3}{\sigma_1} \leq R_0$	≤ 0	Fig. 3.3

B. Fracture Prediction

The probability of failure for an element whose stress state is assumed constant is given by eq. 2.57 as:

$$P_{fa} = 1 - \exp\left[-Am_a k_{Ba} \sigma_{emax}^{m_a} \int_0^1 \bar{\omega}\, S_{cr}^{m_a - 1}\, dS_{cr} \right] \qquad 3.13$$

for surface elements and by eq. 2.60 as:

$$P_{fv} = 1 - \exp\left[-Vm_v k_{Bv} \sigma_{emax}^{m_v} \int_0^{\pi/2} \int_0^1 \bar{\omega} \sin\alpha\, S_{cr}^{m_v - 1}\, dS_{cr} d\alpha \right] \qquad 3.14$$

for volume elements, where σ_1 is replaced by σ_{wmax}, then

$$S_{cr} = \frac{\sigma_{cr}}{\sigma_{emax}}$$

and $\bar{\omega}$ is the probability that a crack will be oriented so that the effective stress is greater than or equal to the critical stress formulated using the appropriate fracture criterion. $\bar{\omega}$ will be a function of two angles β_1 and β_2 and is expressed as:

$$\bar{\omega} = \frac{2(\beta_2 - \beta_1)}{\pi} \qquad 3.15$$

As is the case for the maximum effective stress, $\bar{\omega}$ is dependent on the nature of the stress on an element and is

different for the normal stress which is compressive, tensile or compressive and tensile combined.

1. Compressive loading.

$\bar{\omega}$ is reformulated using the fracture criterion for $\sigma_n < 0$, given in eq. 3.2. Substituting

$$\tau^2 = |\sigma|^2 - \sigma_n^2$$

into eq. 3.2 gives:

$$\sigma_e = \sqrt{|\sigma|^2 - \sigma_n^2} + \mu\sigma_n \qquad 3.16$$

Using the notation given in Table 3.2 for surface or volume analysis, eq. 3.16 becomes:

$$S_e = \sqrt{T - S^2} + \mu S \qquad 3.17$$

which may be written:

$$(S_e - \mu S)^2 = T - S^2$$

or

$$S_e^2 - 2\mu S_e S + (1+\mu^2)S^2 - T = 0 \qquad 3.18$$

Table 3.2 Notation for volume and surface flaw analysis.

Quantity	Symbol	Surface	Volume
Normal Stress	S	$\frac{\sigma_{na}}{\sigma_{emax}}$	$\frac{\sigma_{nv}}{\sigma_{emax}}$
Traction	T	$\frac{\lvert\sigma_a\rvert^2}{\sigma_{emax}^2}$	$\frac{\lvert\sigma_v\rvert^2}{\sigma_{emax}^2}$
Critical Stress	S_{cr}	$\frac{\sigma_{cr}}{\sigma_{emax}}$	
Critical Stress(Squared)	T_{cr}	$\frac{\sigma_{cr}^2}{\sigma_{emax}^2}$	
Effective Stress	S_e	$\frac{\sigma_e}{\sigma_{emax}}$	
Normal Stress at A	S_A	$\frac{\sigma_{1a}}{\sigma_{emax}}$	$\frac{\sigma_{nA}}{\sigma_{emax}}$
Normal Stress at B	S_B	$\frac{\sigma_{3a}}{\sigma_{emax}}$	$\frac{\sigma_{nB}}{\sigma_{emax}}$
Traction at A	T_A	$\frac{\sigma_{1a}^2}{\sigma_{emax}^2}$	$\frac{\lvert\sigma_A\rvert^2}{\sigma_{emax}^2}$
Traction at B	T_B	$\frac{\sigma_{3a}^2}{\sigma_{emax}^2}$	$\frac{\lvert\sigma_B\rvert^2}{\sigma_{emax}^2}$

The traction and the normal stress are:

$$T = T_B + (T_A - T_B)\cos^2\beta \qquad 3.19$$

$$S = S_B + (S_A - S_B)\cos^2\beta \qquad 3.20$$

Substituting eqs. 3.19 and 3.20 into eq. 3.18 gives:

$$\begin{aligned} &S_e^2 - 2\mu S_e S_B - 2\mu S_e(S_A - S_B)\cos^2\beta \\ &+ (1+\mu^2)S_B^2 + 2(1+\mu^2)S_B(S_A - S_B)\cos^2\beta + (1+\mu^2)(S_A - S_B)^2\cos^4\beta \\ &- T_B - (T_A - T_B)\cos^2\beta = 0 \end{aligned} \qquad 3.21$$

At $S_e = S_{cr}$, $\beta = \beta_{cr}$ and eq. 3.21 may be rewritten:

$$a\delta^2 + b\delta + c = 0$$

where $\delta = \cos^2\beta_{cr}$, then

$$\begin{aligned} a &= (1+\mu^2)\ (S_A - S_B)^2 \\ b &= -2\mu S_{cr}(S_A - S_B) + 2(1+\mu^2)S_B(S_A - S_B) - (T_A - T_B) \\ c &= T_{cr} - 2\mu S_{cr} S_B + (1+\mu^2)S_B^2 - T_B \end{aligned}$$

then using the quadratic formula:

$$\delta = \frac{-b \pm \sqrt{b^2 - 4ac}}{2a}$$

where δ has two roots, δ_1 and δ_2. $S_e \geq S_{cr}$ over the interval $\beta_{C1} \leq \beta \leq \beta_{C2}$. $\bar{\omega}$ is given as:

$$\bar{\omega} = \frac{2(\beta_{C2}-\beta_{C1})}{\pi} \qquad 3.22$$

where

$$\bar{\omega} = 0 \qquad b^2 - 4ac < 0$$
$$\beta_{C1} = 0 \qquad \delta_1 \geq 1$$
$$\beta_{C2} = \pi/2 \qquad \delta_2 \leq 0$$

then $0 \leq \bar{\omega} \leq 1$. The region inside Mohr's circle and outside of the fracture envelope represents orientations within which cracks must lie in order to initiate fracture as shown in Fig. 3.9. An example of the solid angle Π on a unit sphere for volume distributed cracks is shown in Fig. 3.10.

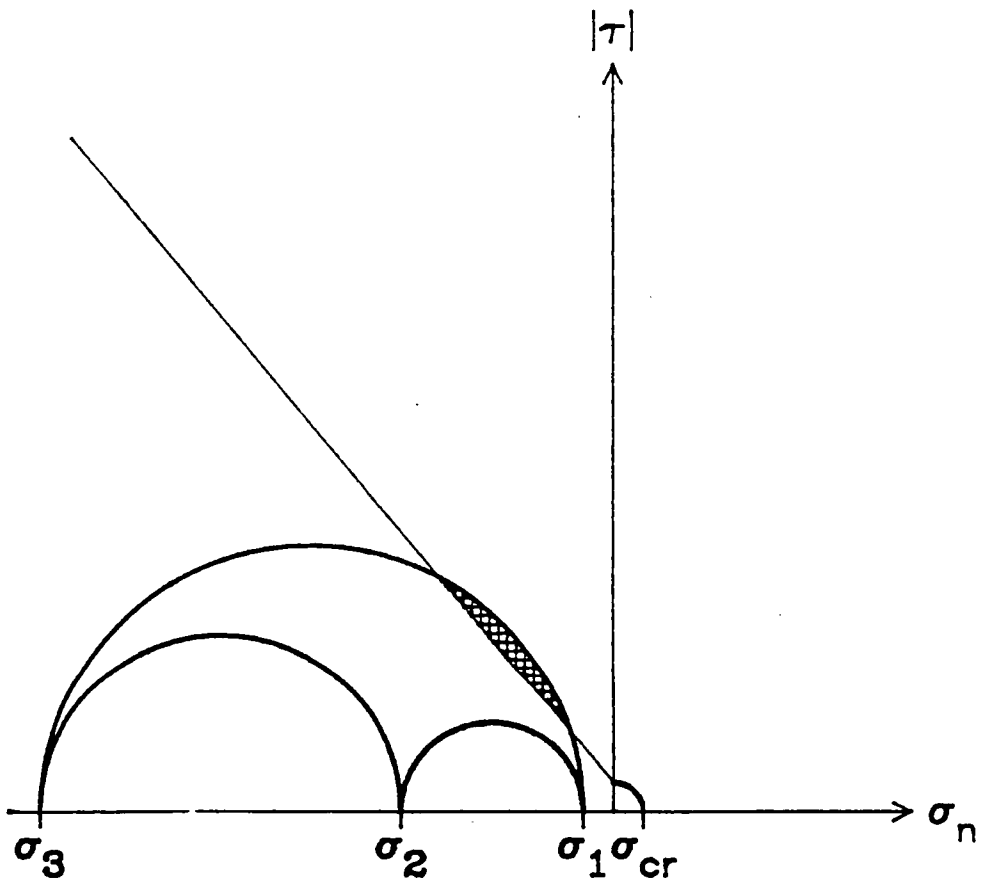

Fig. 3.9 Orientation of cracks which will initiate fracture on Mohr's circle of stress.

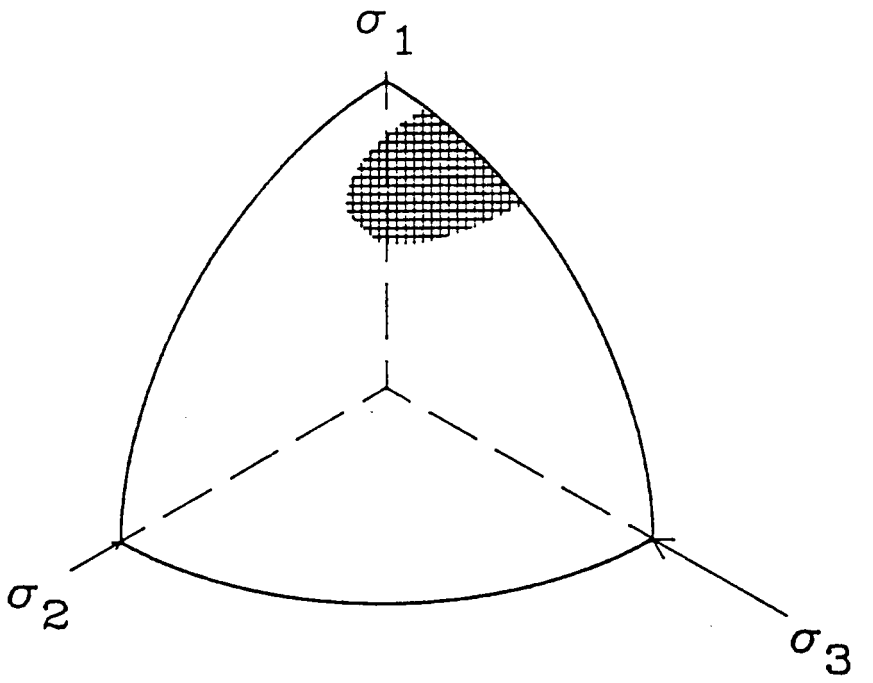

Fig. 3.10 Solid angle within which cracks must be oriented to initiate fracture on a unit sphere.

2. Tensile loading

The probability of failure for surface and volume elements under tensile loading is discussed in Chapter II. To use the general formula for $\bar{\omega}$ given by eq. 3.15, let $\beta_1 = 0$ and $\beta_2 = \beta_T$ where

$$\begin{aligned} \beta_T &= 0 && T_A \leq T_{cr} \\ \beta_T &= \cos^{-1}\left[\frac{T_{cr}-T_B}{T_A-T_B}\right] && T_B < T_{cr} < T_A \\ \beta_T &= \pi/2 && T_{cr} \leq T_B \end{aligned} \qquad 3.23$$

T_A, T_B and T_{cr} are defined in Table 3.2 and $\beta_T = \beta_{cr}$ as given by eq. 2.12 for surface elements and eq. 2.34 for volume elements.

3. Combined tensile and compressive loading

In order to compute $\bar{\omega}$ for elements whose loading is both tensile and compressive, the two fracture criteria are needed. The tensile criterion as given by eq. 2.26 is expressed using the notation in Table 3.2 as:

$$S_e = T^{1/2} = [T_B + (T_A-T_B)\cos^2\beta]^{1/2} \qquad 3.23$$

and the compressive criterion is given by eq. 3.17. The range over which the effective stress is greater than or equal to the critical stress is $\beta_1 \leq \beta \leq \beta_2$, where β_1 and β_2

are equal to the appropriate combination of β_T, β_{C1} or β_{C2}. To determine that combination each criterion must be considered separately. The effective stress, S_e, as a function of β is shown in Fig. 3.11a for the tensile region and Fig. 3.11b for the compressive region.

β_1 and β_2 are dependent on the maximum effective stress for either criteria and whether the normal stress is tensile or compressive at that point. For any orientation (α,β) the maximum effective stress is located in the 13-plane, $\alpha = \pi/2$. When $\alpha \neq \pi/2$, the maximum effective stress is not so easily defined. For the tensile criterion the maximum effective stress is equal to $T_A^{1/2}$ or $T_B^{1/2}$, whichever is larger.

For the compressive criterion, the maximum effective stress is determined using Fig. 3.12. Fig. 3.12 shows Mohr's circle relative to a line whose slope is the same as the linear portion of the fracture envelope. By definition, Mohr's circle for the 13-plane has its center at point O, or the average of the minimum and the maximum principal stresses. As α is constant from A to B, (shown in Fig. 2.4) the normal and shear stress (σ_n,τ) comprise an arc of a circle which is concentric with Mohr's circle for the 13-plane. The stress (σ_n,τ) at the orientation of maximum effective stress will be located on the line $\overline{OP}$ as shown in Fig. 3.12 or the point on the arc closest to the line $\overline{OP}$.

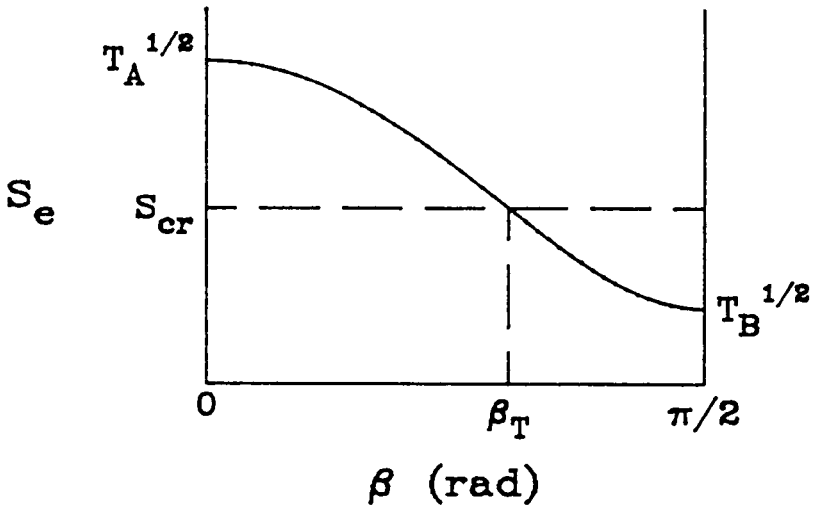

a) TENSILE CRITERION

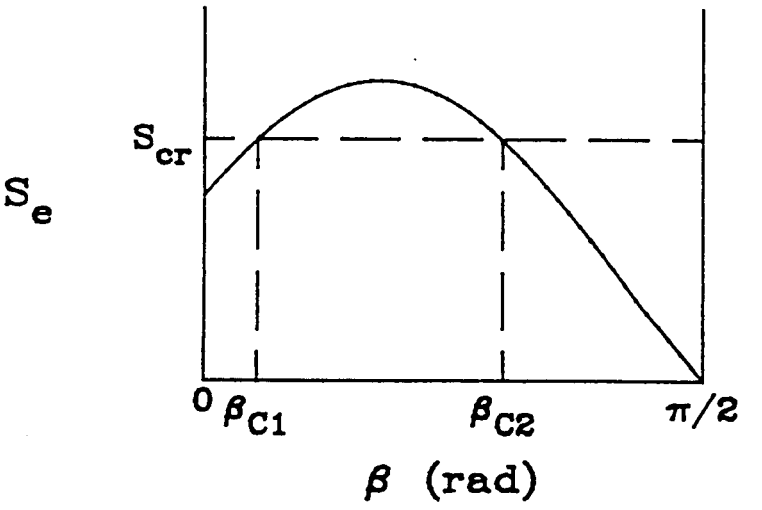

b) COMPRESSIVE CRITERION

Fig. 3.11 The effective stress as a function of crack orientation for A)tensile and b)compressive loading.

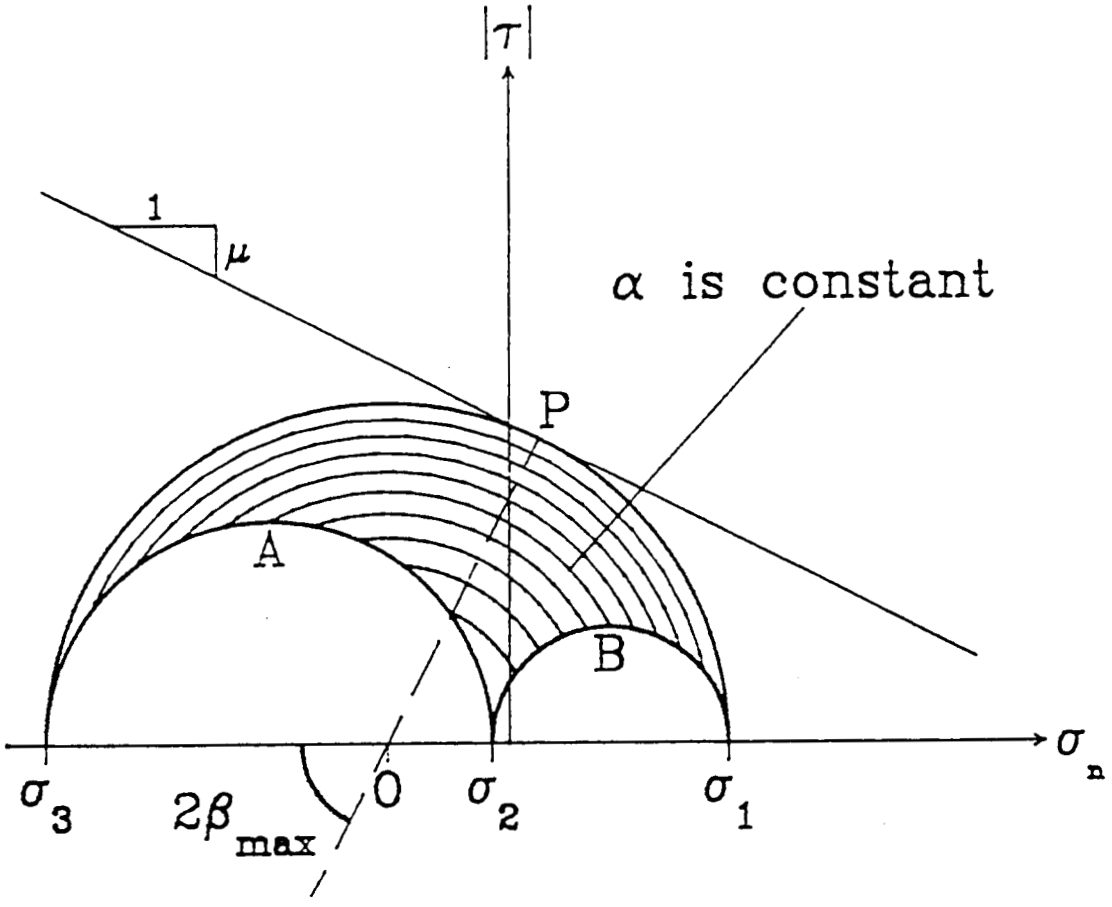

Fig. 3.12 Mohr's circle with the shear as a function of the normal stress for constant α.

The normal stress along $\overline{UP}$ as a function of α is:

$$\sigma_{nm} = R_\alpha \cos 2\beta_{max} + \frac{\sigma_1+\sigma_3}{2} \qquad 3.24$$

where R_α is the radius of the circle on which the arc AB lies and $\cos 2\beta_{max}$ is given by eq. 3.6. If $\sigma_{nB} \leq \sigma_{nm} \leq \sigma_{nA}$, the maximum effective stress is located where $\sigma_n = \sigma_{nm}$ which is on the line $\overline{UP}$. The shear is:

$$|\tau_m| = R_\alpha \sin 2\beta_{max} \qquad 3.25$$

where $\sin 2\beta_{max}$ is given by eq. 3.6. The maximum effective stress is found by substituting eq. 3.24 and 3.25 into eq. 3.2

$$\sigma_{em} = \sqrt{1 + \mu^2}\, R_\alpha + \mu \frac{\sigma_1+\sigma_3}{2} \qquad 3.26$$

$R_\alpha = (\sigma_1-\sigma_3)/2$ if $\alpha = \pi/2$ then $\sigma_{em} = \sigma_{emax}$ for the 13-plane as given by eq. 3.7 If $\sigma_{nB} \geq \sigma_{nm}$, the maximum effective stress occurs when $\sigma_n = \sigma_{nB}$ and when $\sigma_{nm} \geq \sigma_{nA}$, σ_e is a maximum when $\sigma_n = \sigma_{nA}$. For the example shown in Fig. 3.12 as α approaches zero, $\sigma_{nB} \geq \sigma_{nm}$, the maximum effective stress occurs at $\beta = \pi/2$.

The angles β_1 and β_2 are defined differently for:

- $T_A \geq T_B$ and $\sigma_{nm} \geq 0$, The traction is decreasing as β increases and the normal stress is tensile when the effective stress is maximum in compression.

- $T_A \geq T_B$ and $\sigma_{nm} < 0$, The traction is decreasing as β increases and the normal stress is compressive when the effective stress is maximum in compression.

- $T_A < T_B$ and $\sigma_{nm} \geq 0$, The traction is increasing as β increases and the normal stress is tensile when the effective stress is maximum in compression.

- $T_A < T_B$ and $\sigma_{nm} < 0$, The traction is increasing as β increases and the normal stress is compressive when the effective stress is maximum in compression.

An example of the first case $T_A \geq T_B$ and $\sigma_{nm} \geq 0$, is shown in Fig. 3.13. Let $S_e = S_{cr}$, then β_1 and β_2 are:

$$\begin{aligned} \beta_1 &= 0 \\ \beta_2 &= 0 && T_A^{1/2} \leq S_{cr} \\ \beta_2 &= \beta_T && T_0^{1/2} \leq S_{cr} < T_A^{1/2} \\ \beta_2 &= \beta_{C2} && S_{cr} < T_0^{1/2} \end{aligned}$$

where $T = T_0$ at $\beta = \beta_0$.

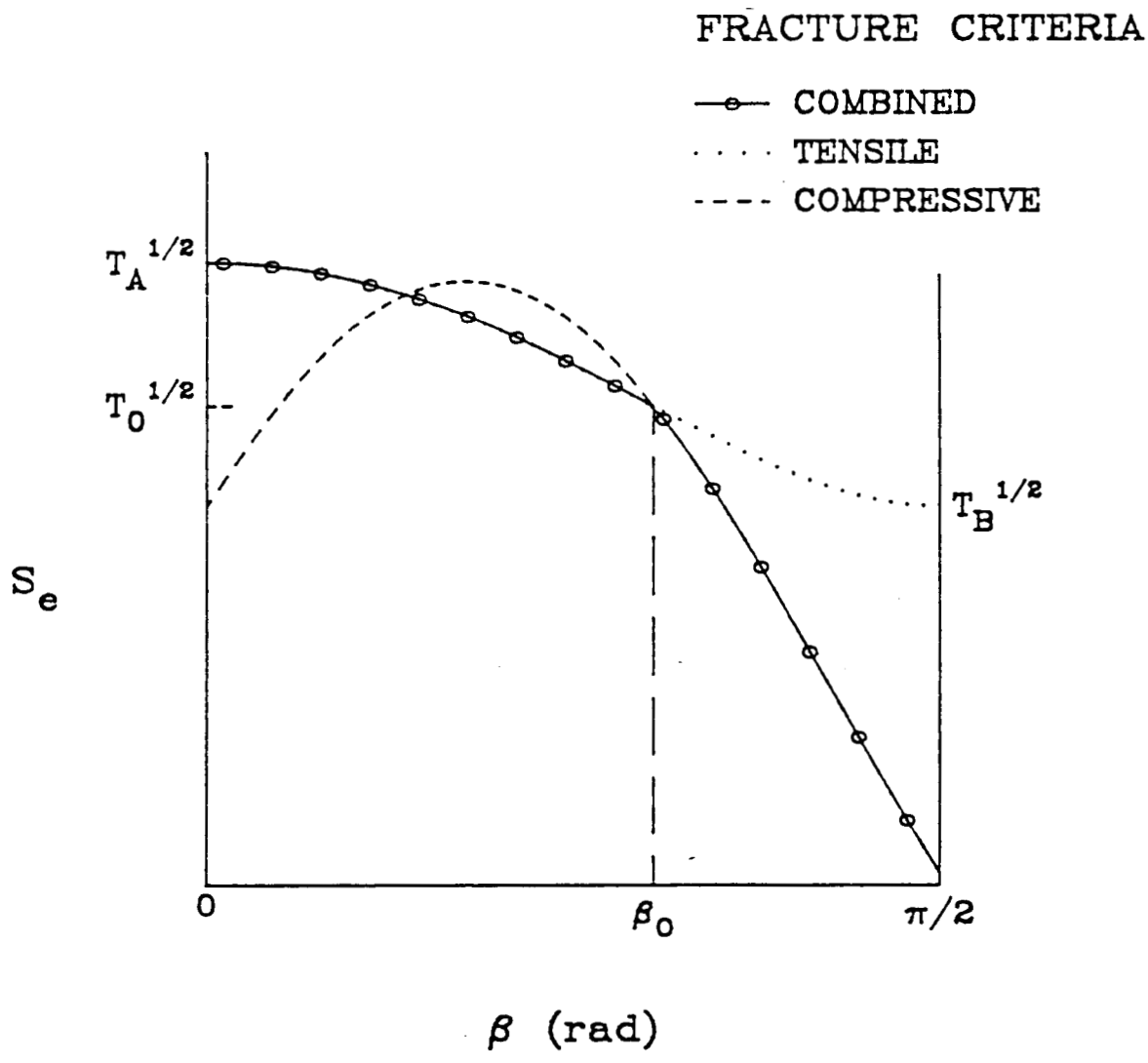

Fig. 3.13 The effective stress as a function of crack orientation, $T_A > T_B$ and $\sigma_{nm} > 0$.

The second case $T_A \geq T_B$ and $\sigma_{nm} < 0$, is physically impossible. Consider the fracture criterion for $S < 0$:

$$S_e = \sqrt{T - S^2} + \mu S$$

if the traction and the normal stress are both decreasing then the effective stress must decrease. When the traction is increasing the effective stress may have a maximum when $S < 0$.

The effective stress as a function of β for the third case $T_A \leq T_B$ and $\sigma_{nm} \geq 0$, is shown in Fig. 3.14. Let $S_e = S_{cr}$, then β_1 and β_2 are:

$$\begin{aligned}
&\beta_1 = 0 && T_0^{1/2} \leq S_{cr} \\
&\beta_1 = \beta_T && T_A^{1/2} < S_{cr} < T_0^{1/2} \\
&\beta_1 = 0 && S_{cr} \leq T_A^{1/2} \\
&\beta_2 = 0 && T_0^{1/2} \leq S_{cr} \\
&\beta_2 = \beta_{C2} && S_{cr} < T_0^{1/2}
\end{aligned}$$

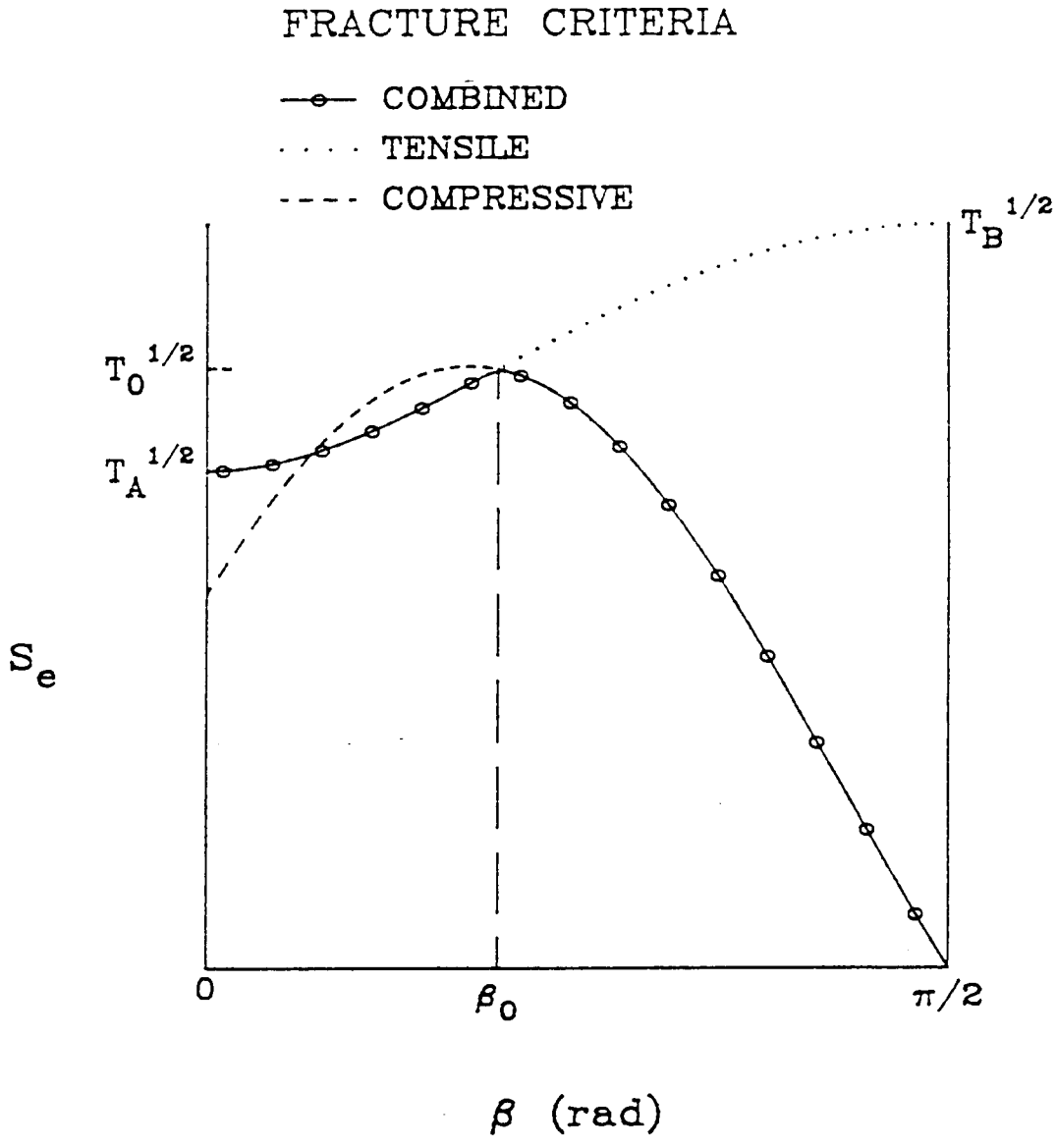

Fig. 3.14 The effective stress as a function of crack orientation, $T_A < T_B$ and $\sigma_{nm} > 0$.

The effective stress as a function of β for the final case $T_A \leq T_B$ and $\sigma_{nm} < 0$, is shown in Fig. 3.15. Let $S_e = S_{cr}$, then β_1 and β_2 are:

$\beta_1 = 0$	$S_{em} \leq S_{cr}$
$\beta_1 = \beta_T$	$T_A^{1/2} < S_{cr} < S_{em}$
$\beta_1 = \beta_{C1}$	$S_{cr} \leq T_A^{1/2}$
$\beta_2 = 0$	$S_{em} \leq S_{cr}$
$\beta_2 = \beta_{C2}$	$S_{cr} < S_{em}$

After computing the probability of failure for an individual element under different loading conditions, these elements are assembled in order to analyze the failure probability for an entire component.

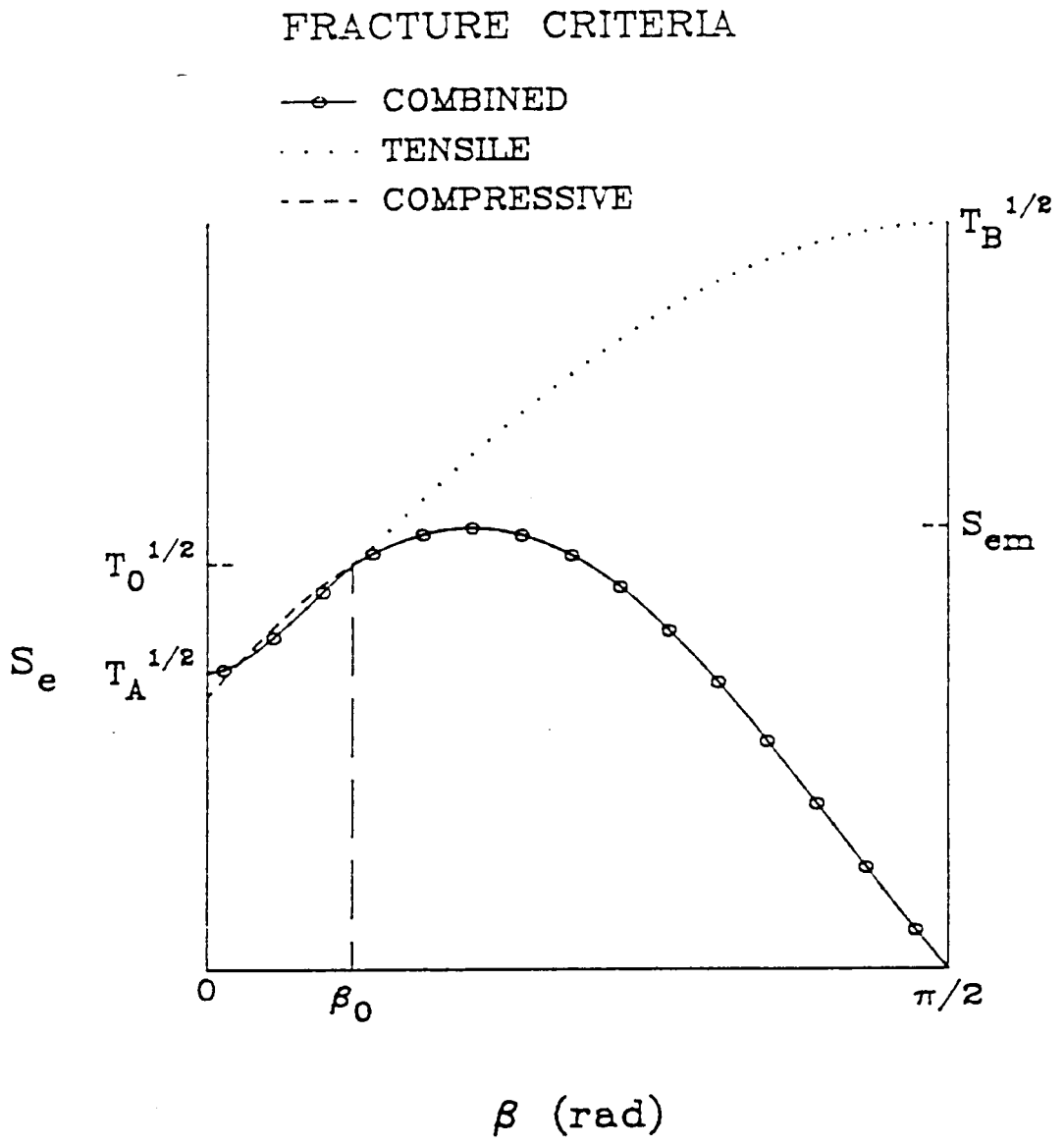

Fig. 3.15 The effective stress as a function of crack orientation, $T_A < T_B$ and $\sigma_{nm} < 0$.

CHAPTER IV

SYSTEM RELIABILITY

The probability of failure for an element of area or volume has been evaluated for tensile or compressive loading in Chapters II and III. In compression, several cracks extend and join together to create a shear fault as shown in Fig. 4.1.[20] To account for the multicracking phenomenon, the material is modeled as a series system rather than independent elements as in the weakest link theory. Reliability analysis is used to correlate the elements and establish bounds on the probability of failure.

A. Finite Element Analysis

This analysis presented to this point has been concerned with evaluating the probability of failure within an element of area or volume where the stress state is assumed constant. To evaluate these stresses the finite element method is used. An element of volume or surface is not the same as an element in "finite element", because its stress distribution may not be assumed constant. The finite

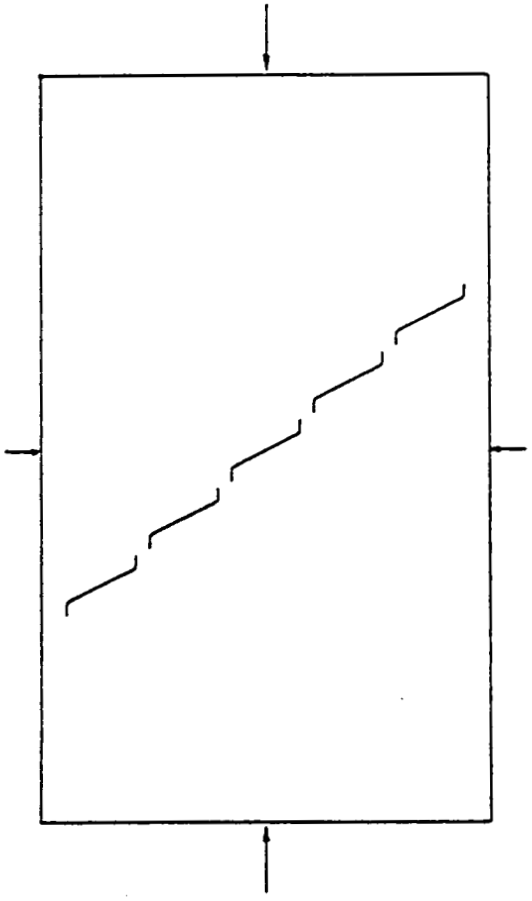

Fig. 4.1 The joining of several cracks to create a shear fault under compressive loading.

element must be divided into sub-elements so that the constant stress assumption is valid. The number of subdivisions is governed by the number of locations at which the stress is output from the finite element program.

Along with the stress at each one of these locations, the area or volume of that sub-element is determined. Finite element analysis makes use of isoparametric elements within which the displacements are formulated using interpolation functions.[27] These interpolation functions enable an element of arbitrary shape in the global coordinate system to be mapped into a natural coordinate system over which the calculations are carried out. The global coordinate system (x,y,z) is representative of the physical system. The natural coordinate system (r,s,t) is constructed so that $-1 \leq r \leq 1$, $-1 \leq s \leq 1$ and $-1 \leq t \leq 1$, The volume of an element is determined using the Jacobian matrix

$$[J] = \begin{bmatrix} \frac{\partial x}{\partial r} & \frac{\partial y}{\partial r} & \frac{\partial z}{\partial r} \\ \frac{\partial x}{\partial s} & \frac{\partial y}{\partial s} & \frac{\partial z}{\partial s} \\ \frac{\partial x}{\partial t} & \frac{\partial y}{\partial t} & \frac{\partial z}{\partial t} \end{bmatrix} \qquad 4.1$$

where for an element with N nodes:

$$\frac{\partial x}{\partial r} = \sum_{i=1}^{N} \frac{\partial h_i(r,s,t)}{\partial r} x_i \qquad 4.2$$

then h_i is the interpolation function and x_i is the global x-coordinate of the ith node. Each term in the Jacobian transformation matrix is computed in the same manner and is a function of r, s and t.

The volume of an element is given by:

$$\iiint_V dV = \int_{-1}^{1}\int_{-1}^{1}\int_{-1}^{1} \left|[J]\right| \, dr \, ds \, dt \qquad 4.3$$

which may be evaluated numerically using eq. 2.55:

$$\iiint_V dV = \sum_{i=1}^{I}\sum_{j=1}^{J}\sum_{k=1}^{K} \left|[J(r_i,s_j,t_k)]\right| \, w_i w_j w_k \qquad 4.4$$

where I, J and K are the number of integration points in the r, s and t directions, respectively. The volume of a sub-element is:

$$V = \left|[J(r_i,s_j,t_k)]\right| \, w_i w_j w_k \qquad 4.5$$

where w_i, w_j and w_k are the weights associated with each sampling point. The number of sub-elements will be equal to the number of integration points used for the element. This technique is appropriate if the stress has been output at the integration points.

The area of a sub-element is determined in the same manner:

$$A = \left|[J(r_i, s_j)]\right| w_i w_j \qquad 4.6$$

where the Jacobian as given by eq. 4.1 is reduced to a 2×2 matrix.

B. Reliability Bounds

Bounds on the probability of failure are determined by considering the elements of a component and their relationship to one another. Before that relationship can be found, the method over which the entire component fails is determined. The fracture of a brittle material will occur when a crack in any part of the component fractures.

This weakest link hypothesis is an example of a series system which is defined in the following way. The component or structure is considered at a fixed point in time, the status of that structure (functioning/failed) is dependent on the states of its elements. The state of an individual elements is expressed in terms of two binary variables, A and B:

$$A_i = \begin{cases} 1 \text{ if element i is functioning} \\ 0 \text{ if element i has failed} \end{cases} \qquad B_i = 1 - A_i \qquad 4.7$$

where i ranges from 1 to k and k is the number of elements in the component. The state of the structure is:

$$A_s = \begin{cases} 1 \text{ if the structure is functioning} \\ 0 \text{ if the structure has failed} \end{cases} \qquad B_s = 1 - A_s \qquad 4.8$$

where A_s for a series system is a function of all of its elements and is given as:

$$A_s = A_1 A_2 \ldots A_k = \min\left|A_1 \ldots A_k\right| \qquad 4.9$$

Substituting eq. 4.8 into 4.9 gives:

$$A_s = A_1 A_2 \ldots A_{k-1} - A_1 A_2 \ldots A_{k-1} B_k$$

Repeating this operation yields:

$$B_s = B_1 + A_1 B_2 + A_1 A_2 B_3 + \ldots + A_1 A_2 \ldots A_{k-1} B_k \qquad 4.10$$

Since the state variables can only take on values of zero or one, it follows that:

$$A_1 A_2 \ldots A_i \geq \max|1 - (B_1 + B_2 + \ldots + B_i), 0|$$

which when combined with eq. 4.10 leads to:

$$B_s \geq B_1 + \sum_{i=2}^{k} \max\left|B_i - \sum_{j=1}^{i-1} B_i B_j, 0\right| \qquad 4.11$$

For any $j \leq i$ it also follows that:

$$A_1 A_2 \ldots A_i \leq A_j = 1 - B_j \qquad 4.12$$

combining eq. 4.10 and 4.12

$$B_s \leq \sum_{i=1}^{k} B_i + \sum_{i=2}^{k} \max_{j<1} B_i B_j \qquad 4.13$$

Bounds on B_s are given by eqs. 4.11 and 4.13 or

$$B_1 + \sum_{i=2}^{k} \max \left| B_i - \sum_{j=2}^{i-1} B_i B_j, 0 \right| \leq B_s \leq \sum_{i=1}^{k} B_i - \sum_{i=2}^{k} \max_{j<1} B_i B_j \qquad 4.14$$

Ditlevsen bounds on P_f are similar to the bounds on B_s as given by eq. 4.14[28]

$$P_1 + \sum_{i=2}^{k} \max \left| P_i - \sum_{j=2}^{i-1} P_{ij}, 0 \right| \leq P_f \leq \sum_{i=1}^{k} P_i - \sum_{i=2}^{k} \max_{j<1} P_{ij} \qquad 4.15$$

where P_i is the probability of failure of an individual element, assembled in decreasing order and P_{ij} is the joint probability of failure of elements i and j. P_1 is equal to the probability of failure for the element with the highest probability of failure. P_{ij} is formulated for simplicity as a function of the safety indices β_i and β_j, given by

$$P_{ij} = P_i P_j + \int_0^{\rho} \varphi(-\beta_i, -\beta_j : z)\, dz \qquad 4.16$$

where

$$\varphi(x,y:\rho) = \frac{1}{2\pi\sqrt{1 - \rho^2}} \exp\left[- \frac{1}{2} \frac{x^2 + y^2 - 2xy\rho}{1 - \rho^2} \right]$$

ρ is the correlation coefficient and the safety index $\beta_i = -\phi^{-1}(P_i)$ is a normally distributed function. The probability of failure as a function of the safety index is shown in Fig. 4.2.

If the correlation coefficient ρ is equal to zero, the elements are not correlated and if $\rho = 1$ they are fully correlated. When ρ is equal to one, a k series system is modeled as one single element whose probability of failure is the average of the k elements.

In order to minimize the size of the problem, the weakest link model is used to combine the sub-elements within an element so that the element may be used to determine the reliability bounds.

The probability of survival is:

$$P_s = 1 - P_f$$

then the probability of survival for the element is:

$$P_s = \prod_{i=1}^{N} P_{s_i} \qquad 4.17$$

where N is the number of sub-elements within an element.

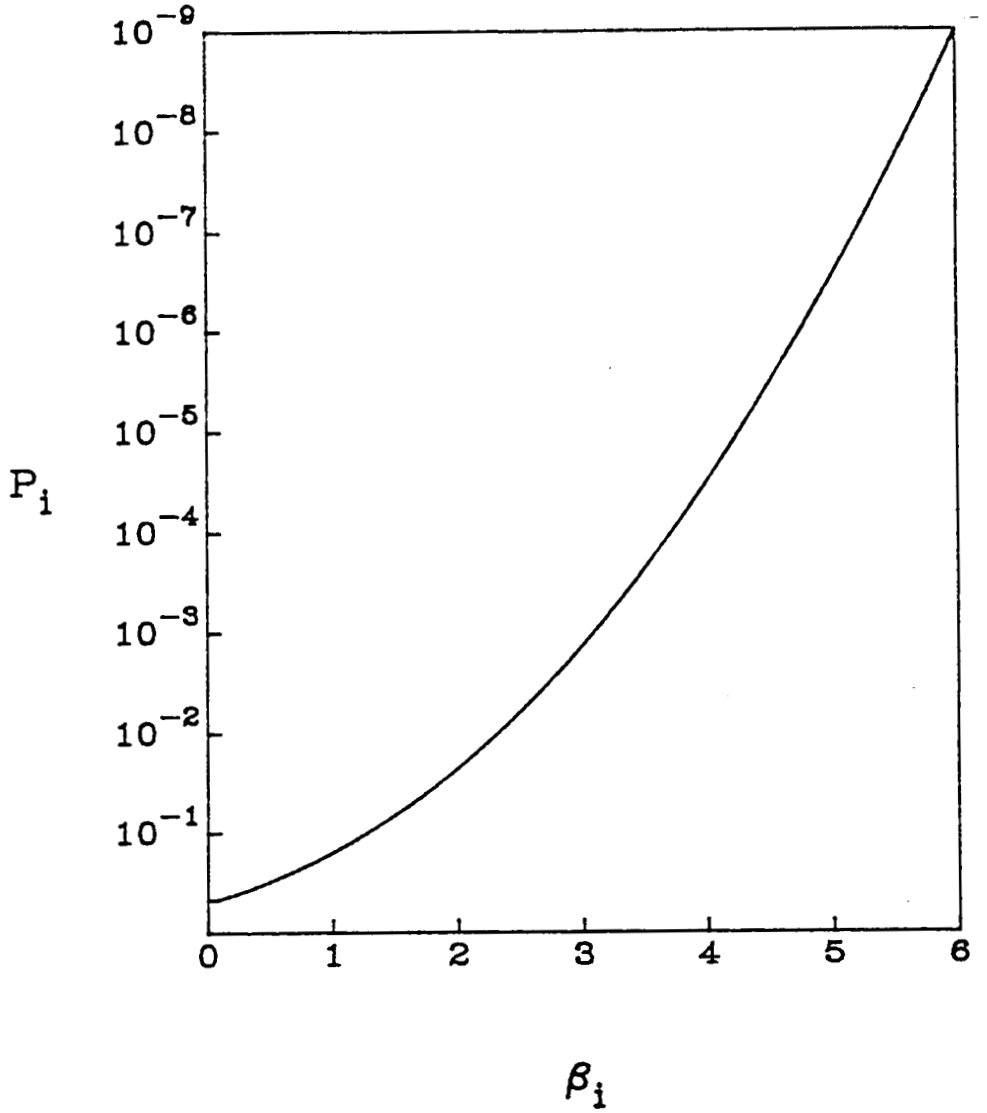

Fig. 4.2 The probability of failure as a function of the reliability index.

CHAPTER V

APPLICATION TO CONTACT STRESS PROBLEMS

The preceding theory is used to evaluate the probability of failure for an alumina ceramic under two different contact stress conditions. First, pressure is applied to two cylinders in contact and second, a compressive load is applied to a beam with a machined notch. The second example is a model of a test conducted at NASA Lewis Research Center where a compressive load was applied to a sample with a machined notch in order to initiate a pre-crack for subsequent studies on fracture toughness. For the first example the stress distribution in closed form is known.[29] However, in general the displacements and stresses are found using the ADINA finite element program.[30]

The material chosen was a 96% alumina ceramic which was used in the experiments at NASA. Three-point bend test data on a beam of circular cross-section was available in the literature[31] and is given in Table 5.1.

TABLE 5.1 Fracture stresses and failure probabilities for 3-point bend specimens.

Fracture Stress σ_f (MPa)	Probability of Failure P_f
378	0.048
417	0.095
421	0.143
430	0.190
448	0.238
453	0.286
455	0.333
457	0.381
461	0.429
470	0.476
472	0.524
475	0.571
479	0.619
493	0.667
495	0.714
497	0.762
502	0.810
528	0.857
532	0.905
540	0.952

The 4-point bend test is preferred because the shear stress between the inner loads is zero. However, the length-to-radius ratio for this beam was large enough so the maximum shear is an order of magnitude less than the maximum normal stress, and is therefore, neglected. The material parameters are calculated from this data and are given in Table 5.2. The dimensions of the beam are given,[32] k and m are calculated using the least squares method and k_{Ba} and k_{Bv} are determined using the technique described in Chapter II.

Table 5.2 Alumina test data.

$R = 0.0016$ m
$L_o = 0.0254$ m
$L_i = 0.$ (3-point bend)
$m = 12.2$
$k = 1.80 \times 10^{-33}$ MPa$^{-12.2}$

$k_{Ba} = 3.99 \times 10^{-27}$ MPa$^{-12.2}$/m^2
$k_{Bv} = 9.72 \times 10^{-23}$ MPa$^{-12.2}$/m^3

The last material parameter necessary for this analysis is the internal friction coefficient. An exact value for this quantity is not known and it must be approximated. The internal friction coefficient is defined as being equal to the slope of the fracture envelope. When the tensile and compressive strengths are known, using simple geometry the friction coefficient is calculated. Using the bend strength of alumina, 315 MPa (45 ksi), and the compressive strength, 2,625 MPa (375 ksi), the internal friction coefficient, μ, is determined and is equal to 1.27.

A. Two Cylinders In Contact

When pressure is applied to two cylinders in contact, (bearings), the region beneath the load is subjected to high compressive stresses. If the displacement in the contact region is assumed to be uniform, a closed form solution for the stress distribution can be found assuming a semi-infinite region.[29] A schematic representation of the applied load on the surface is shown in Fig. 5.1a where p_0 is the maximum pressure at the center of the contact area and a is the half-width of the contact area. The maximum pressure is:

$$p_0 = \frac{2p}{\pi La} \tag{5.1}$$

where p is the applied load and L is the length of the cylinder. The half-width of the contact area is:

$$a = \sqrt{\frac{2p\Delta}{\pi L}} \tag{5.2}$$

where

$$\Delta = \frac{1}{\frac{1}{2}\left[\frac{1}{R_1} + \frac{1}{R_2}\right]} \left[\frac{1-\nu_1^2}{E_1} + \frac{1-\nu_2^2}{E_2}\right]$$

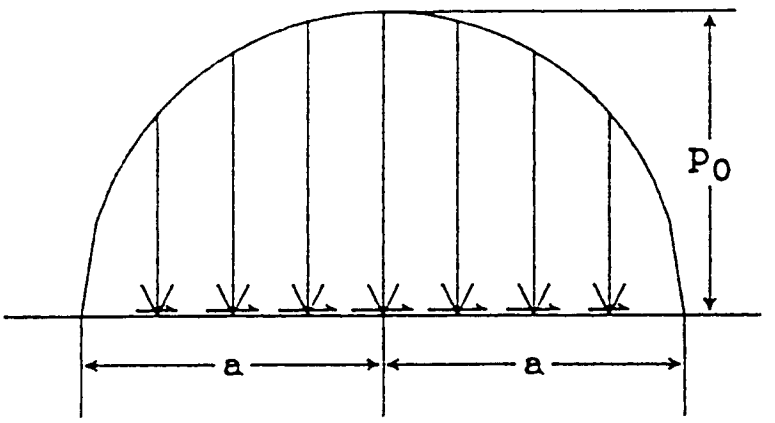

a) The normal and shear load on the boundary

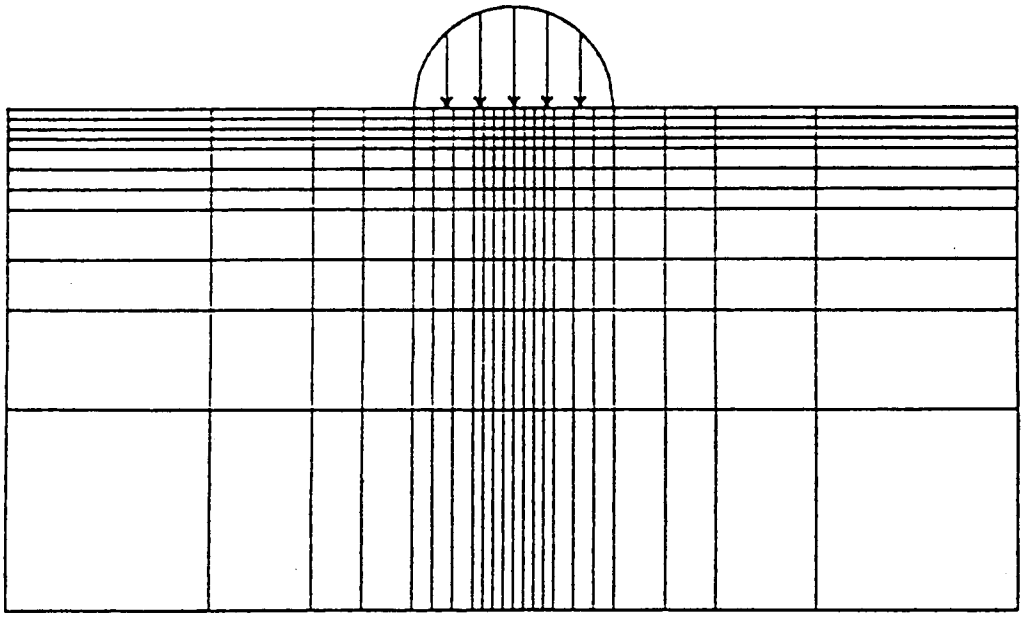

b) Mesh

Fig. 5.1 Schematic view of a contact stress distribution on a semi-infinite region.

where R_1, ν_1 and E_1 are the radius, Poisson's ratio and Young's modulus of the first cylinder and R_2, ν_2 and E_2 are respective properties of the second cylinder.

A closed form solution is available for this loading configuration, in order to evaluate the failure probability, the stress and the volume/area at discrete points is needed. The mesh used to divide the contact region is shown in Fig. 5.1b. The stress is evaluated at the center of each element. The rectangular area is easily determined, however, as the load increases the width of the contact area increases. To compensate for this increase, the volume/area is calculated as the load increases using eqs. 5.1 and 5.2

$$a = \frac{p_0}{p_{0_i}} a_i \qquad 5.3$$

where p_{0_i} is the initial maximum pressure and a_i is the corresponding half-width of the contact area. The initial load along with the bearing dimensions are given in Table 5.3.

C-2

Table 5.3 Bearing material properties and loading configuration.

Dimensions

$$R_1 = R_2 = 0.01 \text{ m}$$
$$L = 0.01 \text{ m}$$

Material properties

$$E_1 = E_2 = 280{,}000 \text{ MPa}$$
$$\nu_1 = \nu_2 = 0.25$$

Initial loading condition

$$p_i = 82.5 \text{ N}$$
$$a_i = 1.875 \times 10^{-5} \text{ m}$$
$$p_{0_i} = 280 \text{ MPa}$$

A contour map of the maximum effective stress normalized with respect to the maximum pressure is shown in Fig. 5.2. The maximum effective stress is less than zero in the region directly beneath the load. Any cracks located in this area will lock. All cracks on the surface will also lock. The maximum effective stress increases away from the load and away from the surface. The highest fracture probabilities can be expected to occur near the locations of largest maximum effective stress.

The probability of failure as a function of the maximum contact pressure is shown in Fig. 5.3. Bounds on the probability of failure are shown for three different correlation coefficients, $\rho = 0$, $\rho = 1$ and $\rho = \rho(r_{ij})$. When

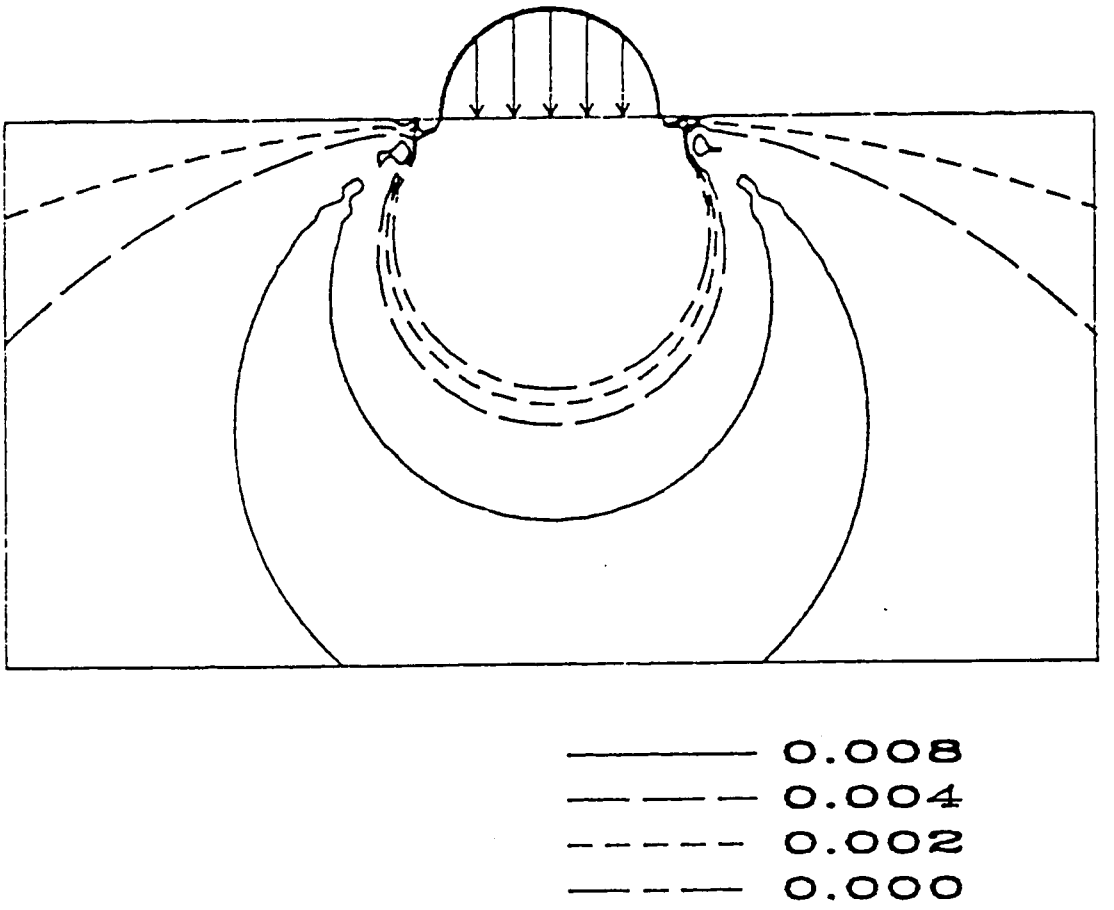

Fig. 5.2 Contours of the maximum effective stress for normal loading only.

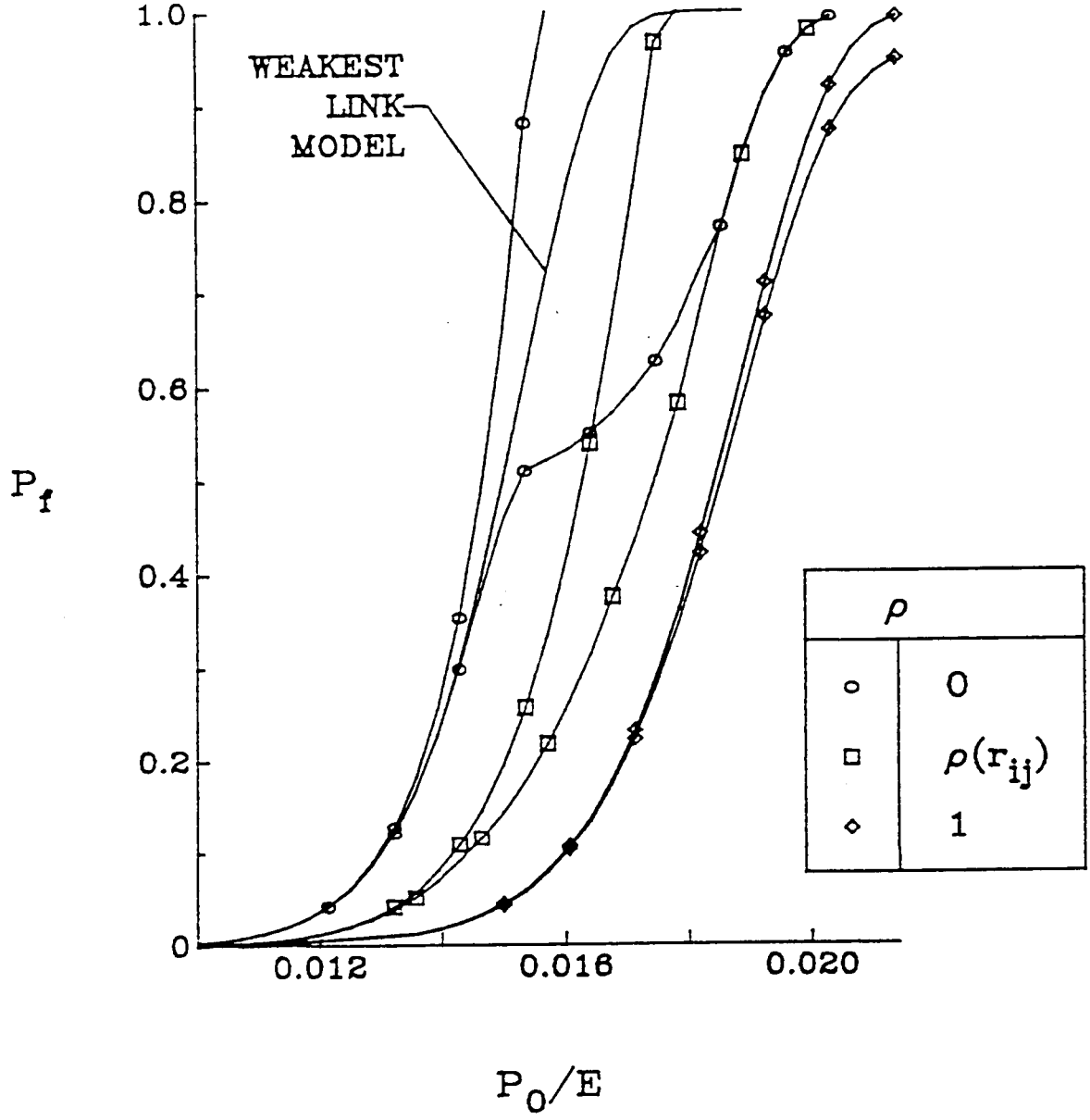

Fig. 5.3 Bounds on the probability of failure as a function of the normalized maximum pressure for different correlation coefficients.

the elements are not correlated, $\rho = 0$, the weakest link probability lies within the Ditlevsen bounds. However, when the system is fully correlated, the probability of failure is substantly lower than the weakest link probability, for a given load. This would indicate that for the whole system to fail more than one element needs to fail. An intermediate correlation function was assumed:

$$\rho_{ij} = \exp - \left[\frac{r_{ij}-c}{c}\right] \qquad r_{ij} \geq c$$
$$= 1 \qquad r_{ij} < c \qquad 5.4$$

where r_{ij} is the distance between the centroids of two elements i and j and c is a constant, usually the average mesh size. This correlation is the most realistic because ρ is equal to one for two adjacent elements and decreases as the distance between elements increases. For this example c was assumed to be equal to one quarter of the width of the contact area or a/2.

The purpose of establishing bounds on the probability of failure is to bracket a narrow range of expected failure probabilities for a given load. Reliability bounds are consistently used for design purposes where $P_f << 1$. As the difference between bounds increases, generally with increasing load, they are not useful for a realistic bounding of the probability of failure. For example, for $\rho = 0$, as the probability of failure exceeds 0.5, the

difference between the bounds increase sharply and the concept of probability of failure is no longer important because failure has occurred.

The largest failure probabilities occur in the area in which the maximum effective stress is greatest as shown by Fig. 5.4, a contour map of failure probabilities for each element. The normalized maximum pressure was 0.0165 when the map was drawn. A crack is most likely to propagate initially in the region of highest maximum effective stress. In practice, cracks originate beneath the surface and then grow around the inside of the bearing parallel to the surface and ultimately, the material peels off. This phenomenon is known as the shell effect.

In the case of roller bearings, a frictional force is acting on the surface in the direction opposite to the relative motion. The tangential load is represented as a fraction of the pressure or

$$q = fp \qquad 5.5$$

where f is the friction coefficient and p is the pressure. A contour map of the maximum effective stress normalized with respect to the maximum pressure for a friction coefficient equal to 0.3 is shown in Fig. 5.5.

As was the case when no friction is present cracks will lock in the area directly below the load. On the surface near the trailing edge of the tangential load the normal

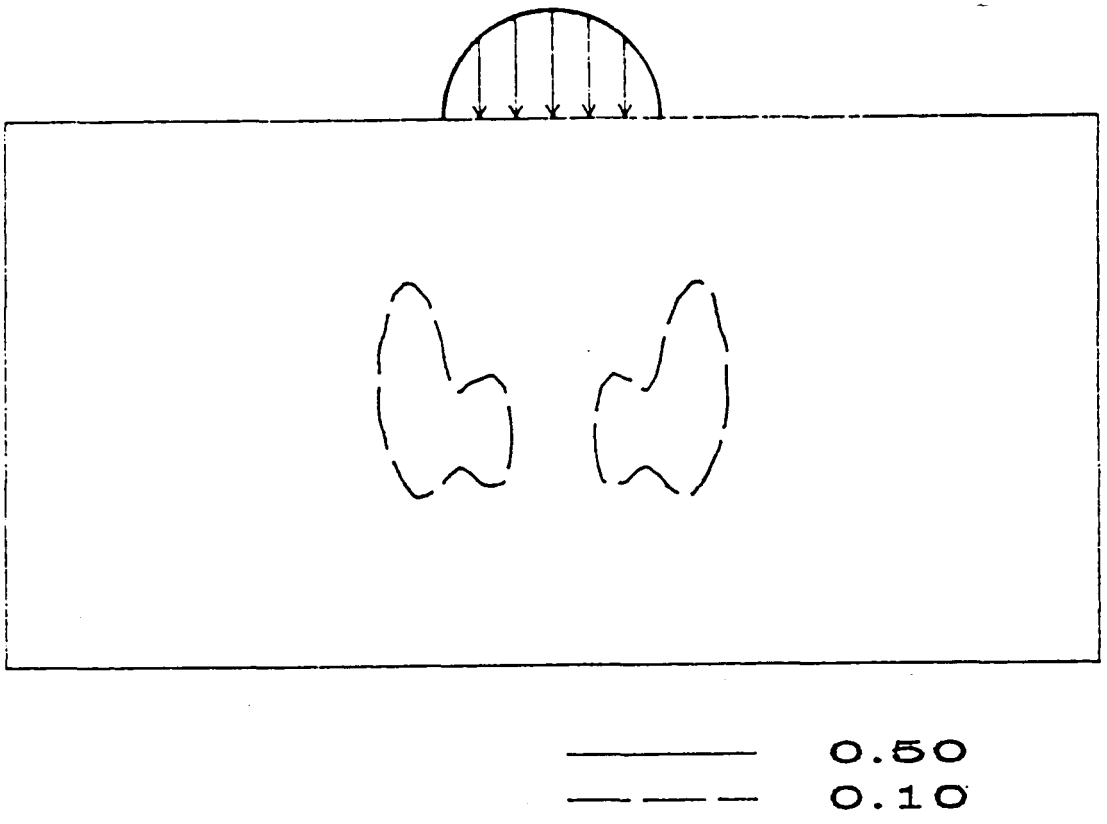

Fig. 5.4 Contour of the failure probabilities for each element.

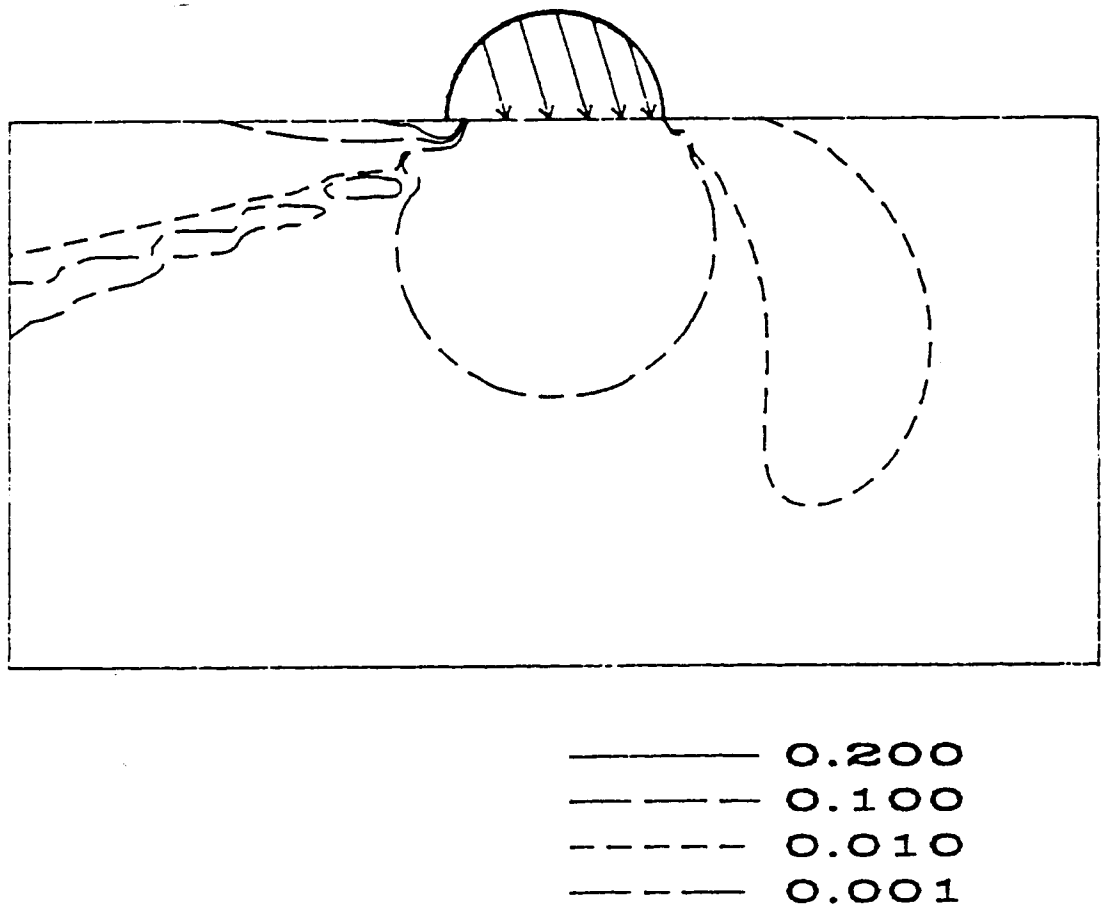

Fig. 5.5 Contours of the maximum effective stress for normal and tangential loading.

stresses are tensile. The maximum effective stress in this area is the largest for the entire map. This dominate area will serve as the most likely place for the propagation of existing cracks. Another maximum on the map also occurs at the leading edge of the load. However, it is not large enough to suspect that failure will occur at that point.

The probability of failure as a function of the normalized maximum pressure is shown in Fig. 5.6. The probability of failure for the entire cylinder is approximately equal to the probability of failure of the element where the maximum effective stress is the highest. The upper and lower bound will converge to that value and are not dependent on the correlation coefficient. Fig. 5.7 shows a contour map of the failure probabilities for each element. A comparison of Figs. 5.5 and 5.7 shows that the region of the highest maximum effective stress is also the region where the probability of failure is the highest.

The probability of failure as a function of maximum normalized pressure is shown in Fig. 5.8 for different friction coefficients. As the friction coefficient increases the tensile stresses near the trailing edge become dominant and the failure probability increases dramatically for a given load.

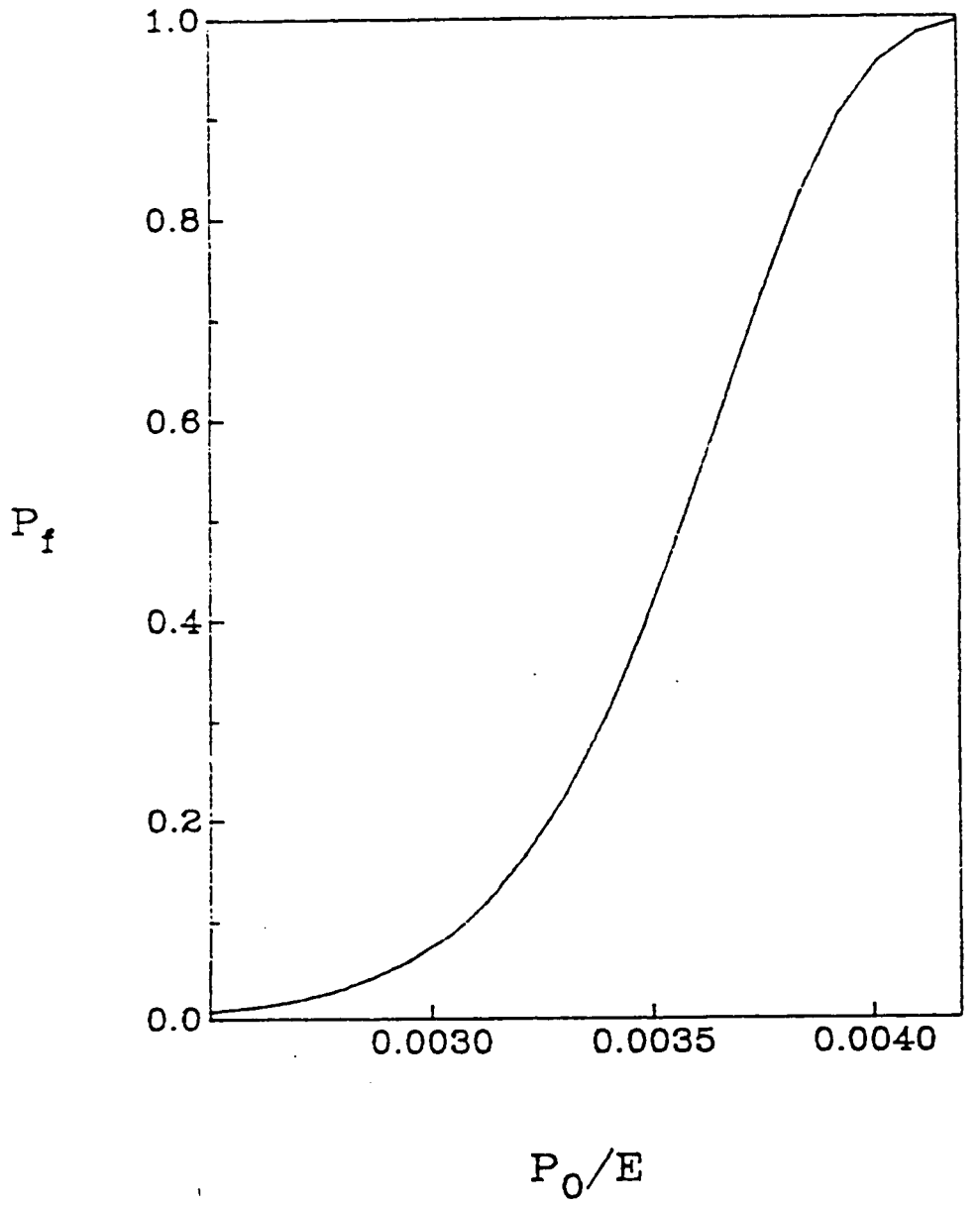

Fig. 5.6 The probability of failure as a function of the maximum normalized pressure with normal and tangential loading.

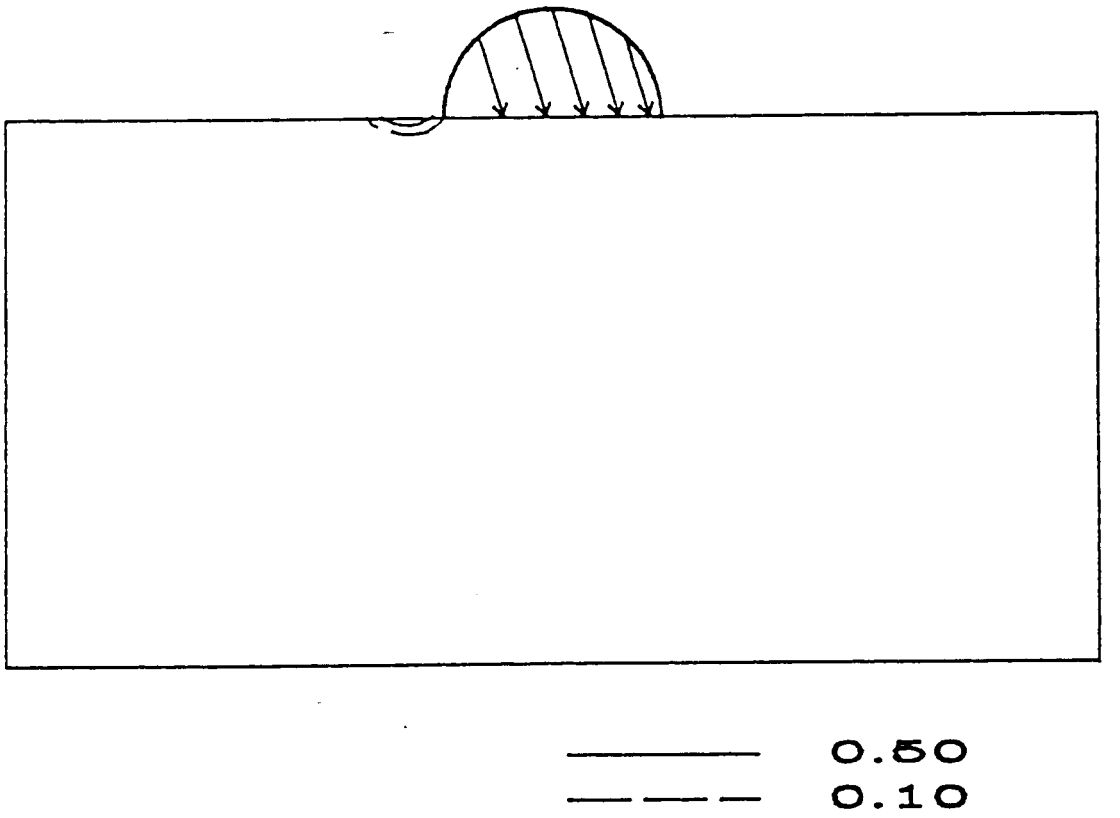

Fig. 5.7 Contour of the failure probabilities for each element.

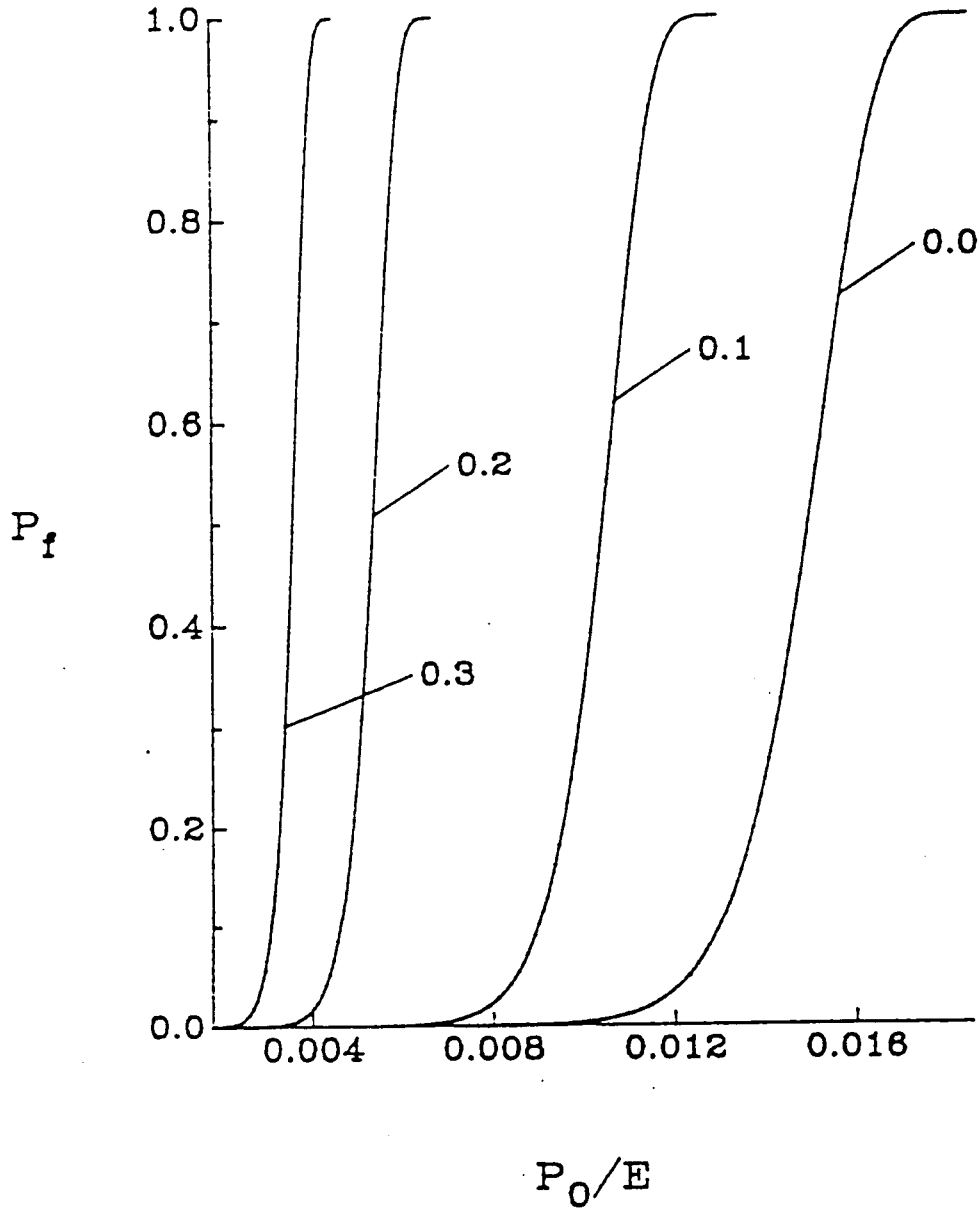

Fig. 5.8 The probability of failure as a function of the maximum normalized pressure for different coefficients of friction.

B. Notched Beam

A test conducted at NASA Lewis Research Center whose purpose was to initiate a pre-crack for subsequent studies on fracture toughness involved applying a compressive load to a beam with a machined notch. The material chosen was a 96% alumina ceramic whose failure data was available in the literature[31] and is given in Table 5.1. The failure stresses found as a result of this analysis are not those expected for this experiment because the sample was fatigued for approximately 10^5 cycles before failure occurred. The purposes of this study were: to determine the location of failure, to define a loading limit under which failure will occur and to suggest a test configuration wherein a single crack grows under compressive loading at the base of the notch.

A schematic showing the beams shape and loading condition is given in Fig. 5.9, where its height, h = 2.5 cm, width, w = 5.0 cm. and the thickness, t = 1.0 cm. The test configuration changed during the course of the experiment. The variable quantities were: the length of the notch, a, the length over which the load is applied, l, and the distance between the back edge of the sample and the point of applied load, d.

Initially, the material was loaded across the entire surface or d = 0, l = w and a = 2.7 cm. A crack was expected to grow at the base of the notch. Fig. 5.10 is a photograph of the beam at failure. After initial small

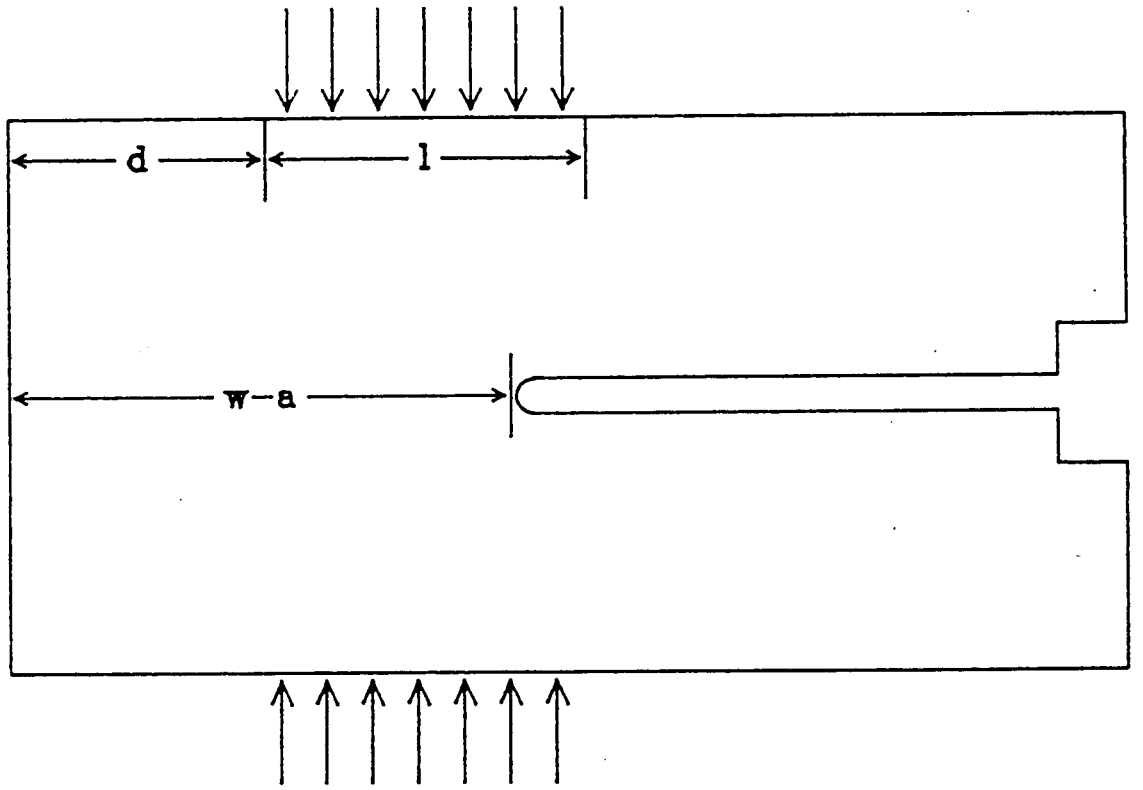

Fig. 5.9 Schematic of the loads applied to the notched beam.

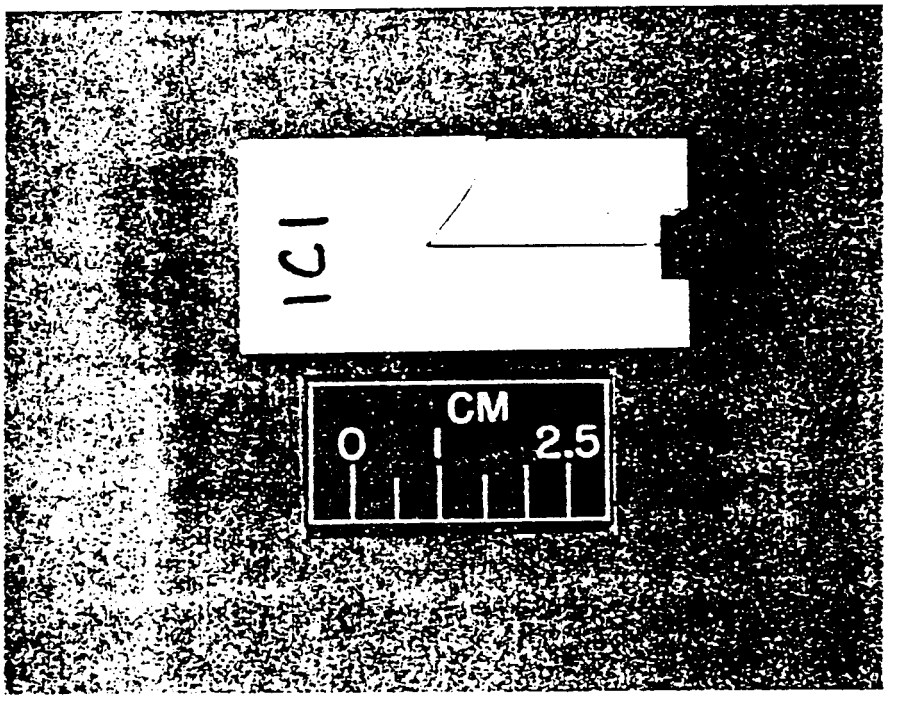

Fig. 5.10 Tensile crack in the notched beam loaded across its entire width.

crack growth at the base of the notch, a second dominant crack originates at the top of the beam. The beam fails in tension. When loading the specimen over three-fourths of its width, ultimate failure still occurs in the form of a tensile crack as shown in Fig. 5.11.

A failure analysis on the beam was conducted by the author in order to determine if the mode of failure was justifyable. The finite element mesh is shown in Fig. 5.12. Because the beam is symmetric about its central axis, only half of the sample was modeled, however the entire beam is considered in the reliability analysis. The finite element model consists of 63 eight-node quadrilateral elements (plane-strain), 230 nodes and 442 nodal degrees of freedom.

After the displacements and stresses were analyzed using ADINA, the stresses and volumes are extracted from the output file and the failure for each element is determined. When the weakest link probability of failure is equal to 0.99, a contour map of the element probabilities of failure is drawn. The map for the beam loaded over its entire width is shown in Fig. 5.13. The element with the highest failure probability is located at the notch tip. However, almost directly above this element at the top of the beam, the region of highest tensile stress is located. The probability of failure in this region is significant in comparison with the failure probability at the notch tip.

This explains the results of the actual experiment. The crack growth initiating at the notch tip is shown by the

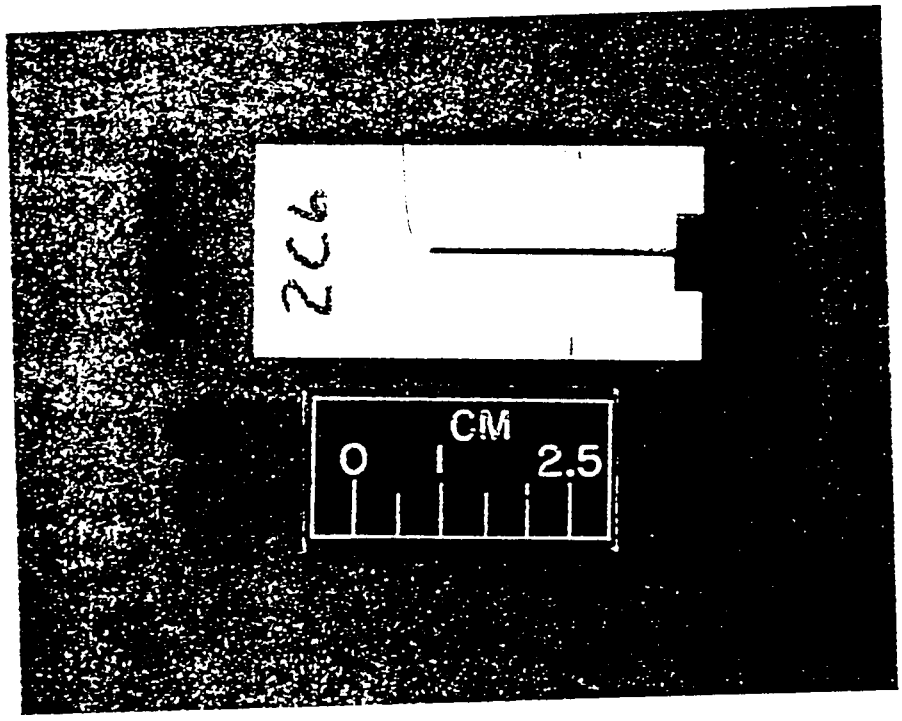

Fig. 5.11 Tensile crack in the notched beam loaded across three quarters of its entire width.

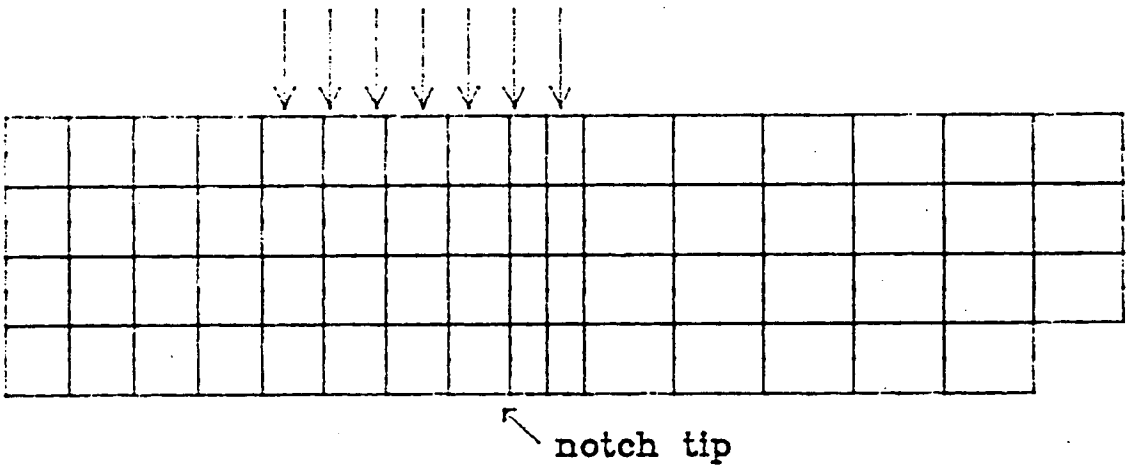

Fig. 5.12 Discretization of the notched beam.

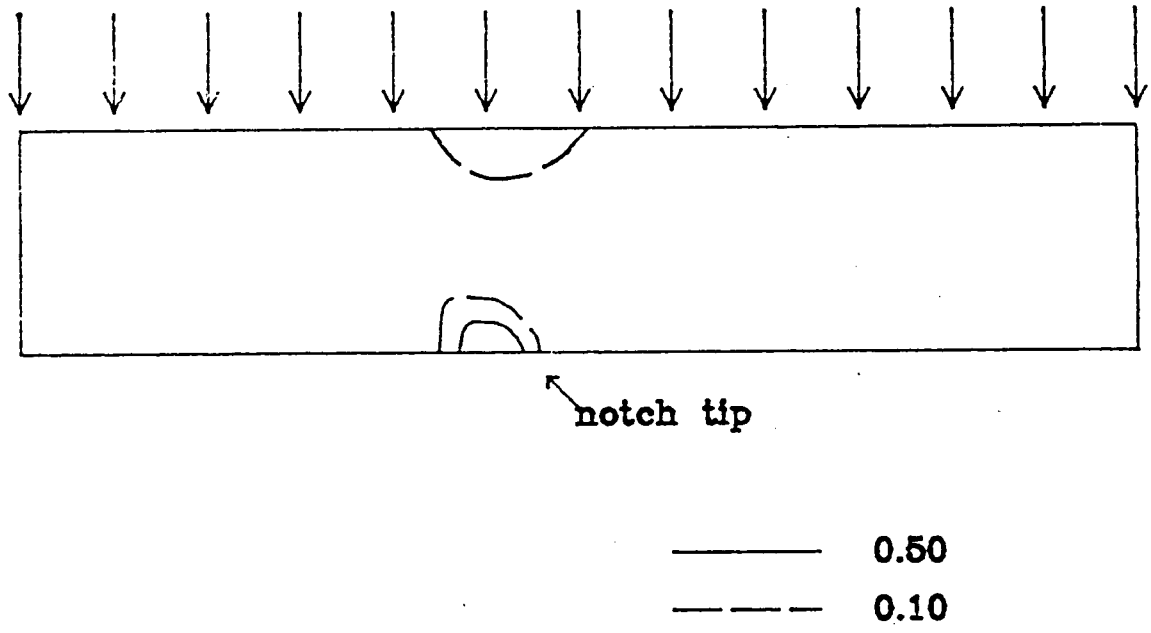

Fig. 5.13 Contour map of the probabilities of failure for the beam loaded over its entire width.

highest probability of failure occurring at that location. Due to the nature of brittle fracture in compression, the crack growth was local. As additional load is applied, the regions of tensile stress will dominate. The tensile crack which breaks the sample is initiated at the top.

Another test was conducted under the following conditions: a = 2.7 cm, l = 1.12 cm, and w = 1.4 cm. The results of the experiment show that a dominant crack initiates in the region of tensile stress. A photograph of that crack is shown in Fig. 5.14. A small crack is initiated at the base of the notch in compression with ultimate failure caused by the tensile crack.

When the weakest link probability of failure is equal to 0.99, a contour map of the failure probabilities for individual elements is shown in Fig. 5.15. The probability of failure is the largest for the element at the notch tip, however at the top of the beam away from the notch, the probability of failure is significant for the tensile stress region.

Fig. 5.16 shows the probability of failure as a function of the applied load. The weakest link probability is shown along with the bounds for three correlation coefficients, $\rho = 0$, $\rho = 1$ and $\rho = \rho(r_{ij})$ as given by eq. 5.4 with c = 0.3 cm. When the elements are not correlated, $\rho = 0$, the weakest link probability is approximately equal to the Ditlevsen bound, yielding a unique solution. However, when the system is fully

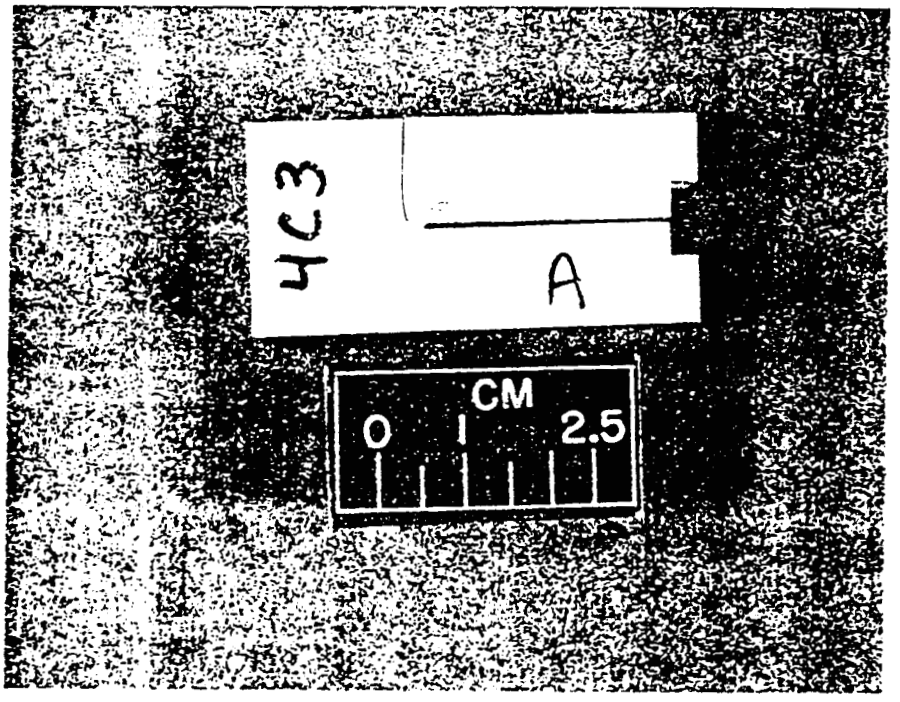

Fig. 5.14 Tensile crack in the notched beam loaded across a section of its entire width.

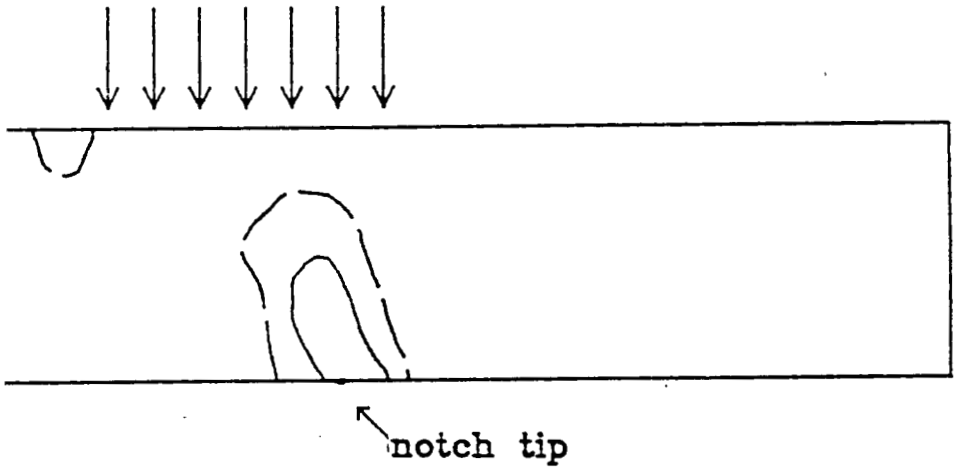

ntour map of the probabilities of failure for as a
e beam loaded over a section of its entire erent
dth.

correlated, the difference between the bounds is substantly greater than for an uncorrelated system. The spread between the bounds for the intermediate correlation coefficient lies between that for a fully correlated and uncorrelated system for a given load. These trends are the same as those found for the cylinders in contact as given by Fig. 5.3.

With an applied load of 44.5 kN (10,000 lbs) the tensile crack appears after 97,320 cycles. This load is approximately 80% of the load required to yield a probability of failure of 0.01 for the weakest link model as shown in Fig. 5.16.

In order to determine a test configuration wherein a crack grows at the base of the notch, a sensitivity study of the possible loading configurations was completed. With the beams height to width ratio of 0.5, an improved test condition was not found. However, if the height was doubled, the tensile stresses away from the notch decrease. Then the probability of failure in these regions will decrease. A contour map of the probabilities of failure of a beam loaded as follows: a = 2.7 cm, l = 1.12 cm, and w = 1.4 cm is shown in Fig. 5.17. The height of this specimen is doubled, h = 5.0 cm. The probability of failure in the elements away from the notch tip has decreased.

The probability of failure as a function of the applied load for the two different heights(identical loading conditions), is shown in Fig. 5.18. For a given load the failure probability decreases for the beam with h = 5.0 cm.

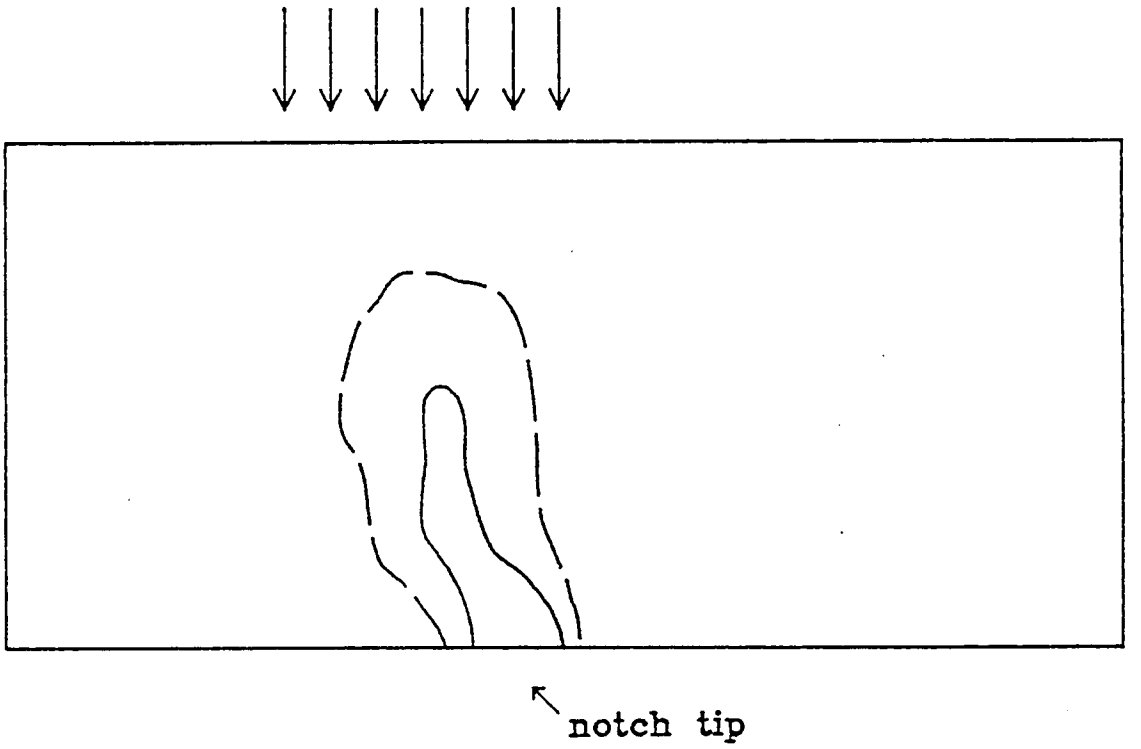

Fig. 5.17 Contour map of the probabilities of failure for the beam loaded over a section of its entire width where the height is doubled.

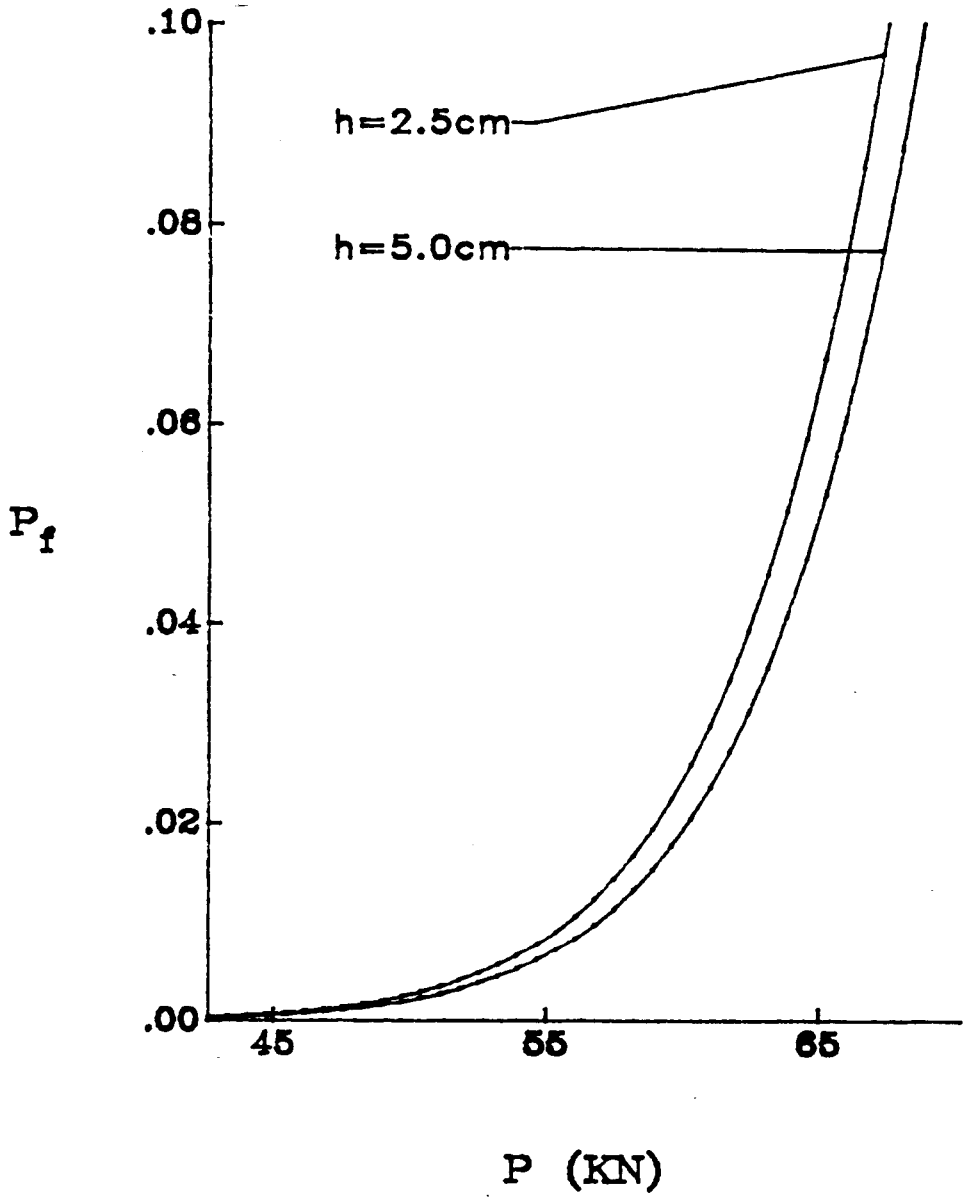

Fig. 5.18 The weakest link probability of failure as a function of the applied load for different beam heights.

The tensile stress in the beam decreases. The volume or the surface area increases for the beam whose height is greater. The combined effect of the two results is the lowering of the probability of failure at a given load for the beam which is larger.

In conclusion, after analyzing the probability of failure for different loading conditions and beam heights, the configuration which would most likely result in crack growth at the notch tip and not in tension is given in Table 5.4. Since the probability of failure decreased for this specimen at a given load, the load which was applied in the earlier experiments may be increased slightly or the number of cycles needed for compressive failure at the notch tip may be increased without the risk of remote tensile failure.

Table 5.4 Dimensions and loading condition of the notched beam.

Dimensions

width	= 5.0 cm (1.92 in.)
height	= 5.0 cm (1.92 in.)
thickness	= 1.0 cm (0.40 in.)
a	= 2.7 cm (1.064 in.)

Loading condition

d	= 1.12 cm (0.44 in.)
l	= 1.40 cm (0.55 in.)
Applied load	= 44.5 kN (10,000 lbs)

CHAPTER VI

CONCLUSIONS

A. Summary

The objective of this study was to analyze the reliability of brittle materials under contact stress conditions. The analysis has shown the following conclusions:

- The failure of brittle materials whose compressive strength is much larger than its tensile strength, is analyzed using a Batdorf model modified to include the reduction in shear due to the effect of the compressive stresses on the crack face.

- Fracture of brittle materials is modeled as a series system.

- As the system becomes more fully correlated the probability of failure decreases for a given load.

- The spread of the bounds increases as the correlation coefficient increases.

- The nature of brittle crack growth in compression results in local crack growth. The presence of a similar crack in tension will lead to catastrophic failure. Failure

of brittle materials is biased in tension.

- The probability of failure is largest in the regions where the maximum effective stress is greatest.

B. Further Work

- A reliability analysis including both the effect of the shear and crushing compressive crack growth mechanisms should be considered.

- An experimental study should be conducted to determine the internal friction coefficient as it relates to characterizing the crack density function for brittle materials.

- Nonlinear fracture envelopes should be applied in examining the reliability of brittle materials under compressive loading.

REFERENCES

1. Boulet, J.A.M.: An Assessment of the State-of-the-Art in Predicting the Failure of Ceramics. Oak Ridge National Laboratory, 1988.

2. Cotterell, B.: The Paradox Between the Theories for Tensile and Compressive Fracture. Int. J. of Fract. Mech., vol. 5, 1969, pp. 251-252.

3. Tracy, P.G.: Rich, T.P.: Bowser R.: and Tramontozzi, L.R.: On the Statistical Nature of Fracture. Int. J. of Fracture, vol. 18, no. 4, 1982, pp. 253-277.

4. Weibull, W.: A Statistical Theory of the Strength of Materials. Ingeniors Vetenskaps Akademien Handlinger, vol. 151, 1939, pp. 5-45.

5. Weibull, W.: A Statistical Distribution Function of Wide Applicability. J. of Appl. Mech., vol. 73, no. 3, 1951, pp. 293-297.

6. Daniels, H.E.: The Statistical Theory of the Strength of Bundles of Threads. I. Proc. Roy. Soc.(London) Series A, vol. 183, 1945, pp. 405-435.

7. Weil, N.A.: and Daniel, L.M.: Analysis of Fracture Probabilities of Nonuniformly Stressed Brittle Materials. J. Am. Ceram. Soc., vol. 47, no. 6, 1964, pp. 268-274.

8. Shih, T.T.: An Evaluation of the Probabilistic Approach to Brittle Design. Eng. Fract. Mech., vol. 13, no. 2, 1980, pp. 257-271.

9. Matthews, J.R.: McClintock, F.A.: and Shack, W.J.: Statistical Determination of Surface Flaw Density in Brittle Materilals. J. Am. Ceram. Soc., vol. 59, no. 7-8, 1976, pp. 304-308.

10. Evans, A.G.: and Jones, R.L.: Evaluation of a Fundamental Approach for the Statistical Analysis of Fracture. J. Am. Ceram. Soc., vol. 61, no. 3-4, 1978, pp. 156-160.

11. Evans, A.G.: A General Approach for the Statistical Analysis of Multiaxial Fracture. J. Am. Ceram. Soc., vol. 61, no. 7-8, 1978, pp. 302-308.

12. Freudenthal, A.M.: Statistical Approach to Brittle Fracture. in Fracture H. Liebowitz, ed. vol. 2, Academic Press, New York, 1968, pp. 591-619.

13. Batdorf, S.B.: Some Approximate Treatments of Fracture Statistics for Polyaxial Tension. Int. J. of Fracture, vol. 13, no. 1, 1977, pp. 5-11.

14. Batdorf, S.B.: and Crose, J.G.: A Statistical Theory for the Fracture of Brittle Structures Subjected to Nonuniform States of Stress. J. Appl. Mech., vol. 41, no. 2, 1974, pp. 459-464.

15. Jayatilaka, A.De.S: Fracture of Engineering Brittle Materials. Applied Science Publications, 1979.

16. Batdorf, S.B.: and Heinisch, H.L., Jr.: Weakest Link Theory Reformulated for Arbitrary Fracture Criterion. J. Am. Ceram. Soc., vol. 61, no. 7-8, 1978, pp. 355-358.

17. Batdorf, S.B.: and Heinisch, H.L., Jr.: Fracture Statistics of Brittle Materials with Surface Cracks. Eng. Fract. Mech., vol. 10, no. 4, 1978, pp. 831-841.

18. Gyekenyesi, J.P.: SCARE - A Post-Processor Program to MSC/NASTRAN for the Reliability Analysis of Ceramic Components, Users Manual

19. Hoek, E.: and Bieniawski, Z.T.: Brittle Fracture Propagation in Rock Under Compression. Int. J. of Fract. Mech., vol. 1, 1965, pp. 137-155.

20. Brace, W.F.: and Bombolakis, E.G.: A Note on Brittle Crack Growth in Compression. J. Geophys. Res., vol. 68, no. 12, 1962, pp. 3709-3713.

21. Argon, A.S., et al,: Fracture in Compression of Brittle Solids. National Materials Advisory Board, NMAB-404, 1983.

22. Adams, M.: and Sines, G.: A Statistical, Micromechanical Theory of the Compressive Strength of Brittle Materials. J. Am. Ceram. Soc., vol. 61, no. 3-4, 1978, pp. 126-131.

23. Alpa, G.: On a Statistical Approach to Brittle Rupture for Multiaxial States of Stress. Eng. Fract. Mech., vol. 19, no. 5, 1984, pp. 881-901.

24. Rufin, A.C.: Samos, D.R.: and Bollard, R.J.H.: Statistical Failure Prediction Models for Brittle Materials. AIAA Journal, vol. 22, no. 1, 1984, pp. 135-140.

25. Lowen, A.N.: Davids, N.: and Levenson, A.; Table of the Zeros of the Legendre Polynomials of Order 1-16 and the Weight Coefficients for Gauss' Mechanical Quadrature Formula. Bull. of the Amer. Mathematical Soc, vol. 48, 1942, pp. 739-743.

26. Obert, L.: Brittle Fracture of Rock. in Fracture H. Liebowitz, ed. vol. 7, Academic Press, New York, 1968, pp. 93-155.

27. Bathe, K.J.: Finite Element Procedures in Engineering Analysis. Prentice-Hall, 1982.

28. Madsen, H.O.: Krenk, S.: and Lind, S.C.: Methods of Structural Safety. Prentice-Hall, 1986.

29. Smith, J.O.: and Liu, C.K.: Stresses Due to Tangential and Normal Loads on Elastic Solid with Application to some Contact Stress Problems. J. Appl. Mech., vol. 20, no. 2, June 1953, pp. 157-166.

30. ADINA Users Manual, Adina Engineering, 1984.

31. Gruver, R.M.: Sotter, W.A.: and Kirchner, H.P.: Variation of Fracture Stress with Flaw Character in 96% Al_2O_3. Ceramic Bulletin, vol. 55, no. 2, 1976, pp. 198-204.